Contribution and limits of portable X-ray fluorescence for studying Palaeolithic rock art: a case study at the Points cave (Aiguèze, Gard, France)

Claire Chanteraud, Émilie Chalmin, Matthieu Lebon, Hélène Salomon, Kevin Jacq, Camille Noûs, Jean-Jacques Delannoy, Julien Monney

Version of Record: https://www.sciencedirect.com/science/article/pii/S2352409X21001103
Manuscript_a156d90021f376ab61c23c34e46fac47

Contribution and limits of portable X-ray fluorescence for studying Palaeolithic rock art: a case study at the *Grotte aux Points* (Aiguèze, Gard, France).

Claire Chanteraud,[1] Émilie Chalmin,[1] Matthieu Lebon,[2] Hélène Salomon,[1] Kevin Jacq,[1] Camille Noûs,[3] Jean-Jacques Delannoy,[1,4] Julien Monney[1]

[1]*Univ. Grenoble Alpes, Univ. Savoie Mont Blanc, CNRS, EDYTEM, 73000 Chambéry, France*

[2] *UMR 7194, HNHP, Muséum National d'Histoire Naturelle, Paris*

[3] *Cogitamus Laboratory, 1 ¾ rue Descartes, 75005 Paris*

[4] *Center of Excellence for Australian Biodiversity and Heritage*

Abstract (100 mots max = 96)

Analysing the colouring matter used to make prehistoric rock art is essential in order to retrace the *chaînes opératoires* involved. Despite the well-documented limitations of portable analysis systems, the need to conserve rock art led us to reassess the capabilities of portable X-ray fluorescence (pXRF) spectrometry. Thus, we compared in-situ and laboratory analyses of materials from the *Grotte aux Points* (France), and laboratory pXRF results with analyses obtained using other methods and with reference samples. Results confirmed that current pXRF systems are unable to provide data suitable for elucidating the *chaînes opératoires* of ferruginous colouring matter.

Keywords: pXRF, PIXE, colouring matter, iron oxide, non-invasive analysis, rock art, Upper Palaeolithic, Gorges de l'Ardèche, France

Highlights

- *Investigation of the limitations of portable X-ray fluorescence spectrometry for analysing prehistoric colouring matter in caves*
- *New approach to analysing pXRF spectra in order to better understand the signals obtained*
- *Petrographical inspection is a crucial first step before geochemical analysis*
- *Testing of quantification models with iron-rich samples and geological standards*
- *Evaluation of the potential for using pXRF to analyse prehistoric rock art and raw colouring matter*

Author credits

Claire Chanteraud: Conceptualisation; investigation; **writing - original draft; formal analysis; data curation; visualization**

Émilie Chalmin: Writing - review and editing; supervision; funding acquisition

Matthieu Lebon: Investigation; writing - review and editing

Hélène Salomon: Conceptualisation; writing - review and editing

Kevin Jacq: Formal analysis

Camille Noûs collective: Methodology; conceptualisation; resources; writing - review and editing

Jean-Jacques Delannoy: Writing - review and editing; supervision; funding acquisition

Julien Monney: Resources; project administration; writing - review and editing; funding acquisition

Graphical abstract

PLEASE INSERT THE GRAPHICAL ABSTRACT HERE

1. Introduction

Because past humans used a wide variety of colouring matter when creating rock art, how and where they collected raw materials, and how they prepared and applied colouring matter, are key questions when contextualising this art. Studying colouring matter can help answer these questions and thereby throw light on the technical and cultural factors that governed the choices past humans made when drawing or painting on rock faces (Salomon 2018). The most common minerals used to make rock art include iron oxide (red hematite) and iron (hydr)oxide (yellow to brown goethite), which occur in numerous geological settings and rock types, including sedimentary rocks (sandstones, oolitic ironstones, limestones) and rocks produced by continental weathering (weathered dykes, ferruginous crusts, bauxites, etc.). Iron-rich colouring matter has been found in many Middle Palaeolithic (Mousterian) to Neolithic sequences, and even at historic sites. It may be unmodified or processed—shaped into millimetre- to decimetre-sized blocks (e.g. Defrasne et al. 2019; Dayet et al. 2016; Pradeau et al. 2016; Salomon et al. 2012) or ground into powder—, or found as applied substances (e.g. Chiotti et al. 2014; Chalmin et al. 2003; d'Errico et al. 2016; Rifkin et al. 2016; Henry-Gambier 2008; Leroi-Gourhan & Allain 1979).

In order to identify the source of archaeological colouring matter, its petrographical and chemical signatures have to be identified and compared with the signatures of potential raw materials (Velliky et al. 2019; Dayet et al. 2016; Pradeau et al. 2016; Mathis et al. 2014; Salomon et al. 2012; Eiselt et al. 2011; Popelka-Filcoff et al. 2007). However, few studies have attempted the much more difficult task of comparing colouring matter and powder applied to walls (Chanteraud et al. 2019; Defrasne et al. 2019; Lebon et al. 2018; Beck et al. 2011; Chalmin et al. 2004).

Analyses of cohesive colouring matter can be used to establish the geological setting in which the raw material formed, but obtaining such information from pictorial matter on the walls of caves or rock shelters is more complex for a number of reasons. First, grinding, shaping, mixing and application processes will have substantially modified the raw material's physical and chemical characteristics (Rosso et al. 2016; Salomon et al. 2016; Pradeau 2015). Second, the current characteristics of colouring and pictorial matter will depend on any post-depositional processes, either within the sediment or on the walls of the cave. Finally, the desire to preserve the integrity of rock art has resulted in severe restrictions being placed on micro-sampling. Many studies have attempted to overcome this constraint by using portable, non-invasive analysis methods, such as portable X-ray fluorescence (pXRF), as an alternative to sampling (Paillet 2014; Beck et al. 2012; Gay 2015; Gay et al. 2016, 2020; Huntley et al. 2015; Mauran et al. 2019; d'Errico et al. 2016; Pitarch et al. 2014; Sepulveda et al. 2015; Olivares et al. 2013; Huntley 2012; Lebon et al. 2019; Nuevo et al. 2012; Roldàn et al. 2010, 2013). As a result, in-situ analyses of this type are now considered an essential preliminary step before any sampling is authorised.

In addition, previous quantitative analyses of cohesive colouring artefacts based on pXRF data have mostly focused on matter unconnected with rock art (Dayet et al. 2019; Dayet et al. 2013; Goemaere et al., 2016; Moyo et al. 2016; Young 2000), which is less susceptible to environmental alteration. Although pXRF spectrometry has several advantages—it is contactless and non-destructive and has very good detection limits for elements with atomic masses between titanium and tin (Shackley 2010)—it has several

limitations that affect its use in archaeology, including for analysing cave walls and colouring material on cave walls (Liritzis et al. 2011; Huntley 2012; Shackley 2010; Shackley 2012; Speakman & Shackley 2013; Shackley 2018; Calligaro et al. 2019). Given the need to protect the integrity of rock art, we decided to thoroughly test pXRF's ability to identify and quantify elements that can be used to differentiate between different samples of colouring matter and pigmented artefacts, and to produce chemical fingerprints of their geological provenance.

We carried out our study at the *Grotte aux Points* (Aiguèze, southern France), which is part of a complex of Palaeolithic rock art caves along the Ardèche river. In addition to containing several panels decorated with red colouring matter (Monney 2018b), archaeological excavations at the *Grotte aux Points* have uncovered numerous fragments of colouring matter and red-pigmented flakes of rock from the cave walls (Chanteraud et al. 2019).

Given the well-documented limitations of pXRF analyses, we carried out pXRF analyses of two international standards and a local geological reference sample. This final sample is part of the *Pigmentothèque* collection of ferruginous rocks with potential for use as colouring matter, found in France's Ardèche and Gard *départements* (Salomon & Chalmin, 2019). We then compared the results of our pXRF analyses with reference analyses of these samples (see section *3.1 Standards*). In order to understand how a material's composition affects pXRF analyses, we also compared our pXRF analysis results with the results of Proton Induced X-ray Emission (PIXE) analyses of the same samples, and Inductively-Coupled Plasma (ICP) analyses of the international standards.

2. Archaeological setting and samples analysed

The Grotte aux Points is a Palaeolithic rock art site in the *Gorges de l'Ardèche*. Its rock art was discovered in 1993 (Brunel et al. 2008, 2018) and has been the subject of archaeological research since 2011 as part of the "*Datation Grottes Ornées*" project (Monney 2018a). An entrance porch leads to a 100-m-long gallery hollowed out of Urgonian limestone. The rock art is confined to the middle of the gallery and consists of 59 dots (called *points-paumes*), produced by pressing the palm of the hand on the wall (Baffier & Feruglio, 1998), five animal figures (three ibex, a horse and a bison), an angular line, and a few indeterminate marks consisting of single lines and dots (Monney 2018b). Expansion processes (Jaillet & Monney 2018) have caused fragments, some of them pigmented, to flake off the walls, and several flakes bearing red pictorial matter applied with the palm of the hand have been found at the foot of the walls in the *Grands Signes* area.

The Points Cave is today hydrogeologically inactive. Only few infiltrations can be observed after strong precipitation events. The low level of leaching on the wall and the quasi-absence of calcite veil is due to this weak hydrogeological activity. Millimetric to centimetric concretions and efflorescence developed on wall surface in ornated sector (coralloid type of crystallization).

In addition, excavations of the silty-clay sediment in the cave's porch have uncovered remains showing the presence of both humans and animals in the cave (flint, charcoal, colouring matter, animal remains, etc.). On the basis of the flint tool-making style, these remains can be attributed to the Middle Gravettian and, possibly, Solutrean periods

(Boccaccio 2018). Sixty-three, millimetre-sized blocks of red colouring matter have been extracted from these deposits.

The present study was based on three types of colouring matter and pigmented fragments: (i) blocks of solid colouring matter found during excavations of the entrance; (ii) pigmented flakes from the walls of the cave, found at the foot of the *Grands Signes*; and (iii) graphic entities (analysed in situ) in the decorated part of the cave.

2.1. Solid colouring matter in the Grotte aux Points

The blocks of solid colouring matter (N = 63) found during excavations were examined in the laboratory under an optical microscope (OM) and using a scanning electron microscope coupled with an energy dispersive X-ray spectrometer (SEM-EDS). These analyses allowed us to categorize the fragments into five lithologies, although the surfaces of six of the blocks were partly or entirely covered by calcium carbonate crusts (Chanteraud et al. 2019) (Table 2).

Lithology A (38 blocks) is a cohesive, soft, red-to-purple argilo-ferruginous rock (grain size < 63 µm), consisting of a detrital matrix impregnated with iron oxide (hematite). Ten of these blocks present 100- to 200-µm celadonite inclusions. We labelled this variant "lithology Av" (Figure 1).

Lithology B (2 blocks) is a cohesive, brown-to-yellow (goethite) argilo-ferruginous rock with a metallic lustre. The matrix contains silt-sized quartz grains, together with macro-, meso- and micropores, some of which are filled with goethite or calcite (Figure 1).

Lithology C (2 blocks) consists of cohesive blocks of fine-grained colouring matter composed of silt-sized quartz grains cemented by a hematite-rich, argilo-ferruginous matrix. These blocks also contain unfilled micropores (Figure 1).

Lithology D (4 blocks) is a coarse-grained sandstone composed of silt-to-sand-sized quartz grains cemented by well-crystallised hematite and clay minerals. One of the blocks assigned to this lithology contains 100- to 200-µm green inclusions, similar to those found in lithology A. We labelled this variant "lithology Dv" (Figure 1).

Lithology E (1 block) is a black to yellow rock with a concretion-like morphology (presence of successive layers). It consists of silt-to-sand-sized quartz grains cemented by flakes of goethite and clay minerals (<1 µm) (Figure 1).

PLEASE INSERT FIG.1 HERE

2.2 Pictorial matter on wall flakes

The colouring matter on flakes of rock found at the foot of the decorated panels (*Grands Signes*) was deposited in flat patches a few micrometres thick (~100 µm), each with a different hue. These coloured deposits seem to impregnate the surface of the limestone fragments:

- S-ECA-01: orange to dark-red gradation covering almost the entire surface (±7 cm^2).
- S-ECA-02: red over its entire surface (± 2 cm^2) (Figure 2)
- S-ECA-03: red to reddish-brown over an area of ± 10 cm^2 but probably affected by the surrounding sediment.

Macroscopic and microscopic laboratory analyses of flakes of rock from the decorated walls revealed traces of argilo-ferruginous colouring matter, around 20 µm thick and ranging in colour from orange to red. This colouring matter contains silt-sized quartz grains (<63 µm) and iron oxides (Chanteraud et al. 2019).

2.3. Pictorial matter in the Grotte aux Points

Macroscopic field observations of the panels showed differences in the morphologies of the pictorial matter in the different graphic entities (Figure 2):

- The ibex (PTS-04, Figure 3), bison and horse figures on the two animal panels are formed by lines of irregular width (generally a few millimetres), composed of a thick layer (>100 µm) of dark red pictorial matter which sometimes contains black inclusions visible to the naked eye.
- The *Grands Signes* panel (PTS- 09 and 10), the gallery and the *Niche aux Points* are decorated with *points-paumes*, produced by covering the palm of the hand in powdered, red colouring matter and pressing it onto the rock. The resulting layer of pictorial matter is only a few microns thick (Chanteraud et al. 2019).

PLEASE INSERT FIG.2 HERE

3. Standards and methods

3.1. Geological reference samples and international standards

We analysed two international geostandards (under vacuum pressed pellets) from the French Scientific Research Centre's (CNRS) Rocks and Minerals Analysis Department in Nancy (SARM, CRPG UMR 7358 CNRS-UL): DR-N, a diorite with a light matrix composed of 70% aluminosilicate (Al_2O_3, SiO_2), and BX-N, a bauxite with an aluminosilicate matrix (62%) and an iron-oxide-rich (22% Fe_20_3) laterite crust. We also used a local sample, called Bordezac after the locality in which it was found, as a high-iron-content (70% Fe_20_3) reference sample. This sample was taken from an iron-rich hydrothermal vein within a Triassic arkosic sandstone formation (T*i*) and has a comparable chemical composition to the archaeological remains. The sample of Bordezac was prepared as polished cube block with very fine polishing (fine grinding 1/4µm). We used these analyses to assess the reproducibility of pXRF analyses from laboratory to cave.

3.2. ICP analysis

ICP spectrometry provides robust quantification for major elements (quantified using emission spectrometry ICP-OES) and unparalleled detection limits for trace elements (quantified using mass spectrometry—ICP-MS). In addition, it allows accurate and precise quantifications to be made of chemical signatures, so it is frequently used as a reference analysis method. Because the certified compositions of our two international standards (DR-N and BX-N from the CRPG, France) were produced using ICP, we asked the Rocks and Minerals Analysis Department to carry out an ICP analysis of the Bordezac local reference

sample, which they did using an acid digestion protocol and a ThermoFischer ICap 6500 emission spectrometer and ICapQ mass spectrometer.

3.3. PIXE analysis

We assessed the sensitivity and reproducibility of pXRF analysis by comparing pXRF results with those provided by µPIXE spectrometry without preparation of archaeological colouring matter. To do this, we carried out both pXRF and µPIXE analyses of the international standards and the Bordezac reference sample, so we could compare the resulting elemental compositions and individual element-to-iron ratios.

For the µPIXE analyses (beamtime obtained at AGLAE facility, C2RMF, Paris), we used a 10-µm extracted beam and filtered the signal by placing a 50-µm-thick aluminium film in front of the high-energy detectors (HE1, HE2 and HE3), a 13-µm chromium filter in front of HE3, and a 100-µm beryllium filter in front of HE4. As well as minimising the influence of Al, Si, Ca and Fe, these filters reduced pile-up effects caused by elements in the matrix, thereby improving the detection and quantification of trace elements. Detection limits were a few ppm (Mathis et al. 2014). We processed the data by using TRAUPIXE and GUPIX software to apply Pichon et al.'s (2010) spectrum modelling and air extraction under the peaks protocol. Quantification in GUPIX was carried out using a configuration file developed specifically for ferruginous colouring matter (Beck et al. 2012; Mathis et al. 2014).

3.4. pXRF analysis method

3.4.1. Apparatus

For the pXRF analysis, we used an ELIO XGlab portable spectrometer (owned by the HNHP research group - UMR 7194, MNHN) combined with two lasers (focusing) and a digital lens controlled by the ELIO software. Using a 1.2-mm-diameter beam meant that the volume of material analysed was comfortably greater than 1 mm^3. The excitation source was a rhodium anode with a 100 µA current, which gave a 40 kV excitation beam. Spectra recordings showed the X-ray excitation lines of the source: K_α = 20.16 keV, K_β = 22.724 keV, but there was no possible superposition between these lines and those of the elements detected. To ensure there was no contact between the spectrometer and the sample or rock wall, we used a working distance of 1.4 cm, measured by two converging lasers at the focus point. The detector (SDD) had an area of 25 mm^2 with a 4,096-channel resolution. We set the acquisition energy at 40 kV in order to detect elements with atomic masses greater than or equal to that of aluminium. The air space between the sample and the detector prevented us detecting elements with atomic masses lower than aluminium. The argon detected in all the spectra was from the air layer the X-rays had to travel through. The K_β line at 3.19 keV of this element can be confused with the K_α line of potassium (3.31 keV). We set the acquisition time for each point at 300 s in order to reach the counting threshold, which does not improve significantly if analysis times are increased (Mauran et al. 2019). We used the same parameters for all the analyses, whether they were carried out in the cave or in the laboratory.

3.4.2. Difficulties in carrying out analyses in situ

Carrying out pXRF analyses within the cave was not always easy due to difficulties getting the equipment into the cave (size, weight, power source, etc.) and to the complex morphology of the cavities containing the rock art, whose uneven floors and sometimes overhanging and irregular panels (up to 3-m high) made it difficult to position the apparatus correctly (Figure 3).

PLEASE INSERT FIG.3 HERE

Despite these constraints, we managed to conduct 66 analyses within the cave, consisting of 43 analysis points on pictorial matter and 23 points on the bare substrate (non-pigmented limestone) adjacent to the pictorial matter analysis points. We analysed pictorial matter in all 32 graphic entities (21 *points-paumes*, all 3 animals figures and 8 abstract marks), measuring up to three points on each entity (Table 1 and 1bis, supplementary information). We also carried out analyses in the laboratory, measuring 2 points on each block of colouring matter and 20 points on pigmented flakes of rock (10 points on the pictorial matter + 10 points on the bare substrate).

3.5 Data analysis (Matlab, PyMCA)

We used a chemometric approach to investigate the limits and potential of pXRF analysis, focusing directly on pXRF spectra and not on values extracted from the spectra. To do this, we developed a Matlab routine: i) to apply a quadratic function to the raw signal (in channels) and thereby calibrate it to an energy resolved spectrum (0.01 keV resolution), ii) to correct the baseline, and iii) to smooth the background noise by applying a Savitzky-Golay filter (Savitzky & Golay 1964; https://doi.org/10.6084/m9). We applied this routine to all the analyses performed on the cave walls, cohesive colouring matter, international standards and Bordezac reference sample.

For the cave wall analyses (bare wall and pictorial matter), we first visually compared the processed spectra in order to assess the reproducibility of the analyses of the standards and the heterogeneity of the compositions of the pictorial layers and blocks of colouring matter. We then subjected these spectra to a principal component analysis (PCA), with the X photon emission energy values as variables, that is, 4,096 times 0.01 kev (Panchuk et al., 2018; Pearson 1901) in order to identify all the chemical components contained in the spectra. Combining chemiometrics with PCA creates a powerful tool for exploring analysis spectra without losing information (Panchuk et al. 2018).

In the case of the blocks of cohesive colouring matter, we performed a second set of PCAs on the peak areas of elements identified as main components of the colouring material, in order to reduce the number of variables and determine whether it was possible to divide the blocks of colouring matter into groups on the basis of their visual petrographic/lithological characteristics. To do this, we obtained semi-quantitative chemical analyses by identifying the chemical elements present and then using PyMCA software to calculate the areas under the peaks (Solé et al. 2007).

Finally, we compared the elemental compositions provided by the different analysis methods for the two international standards and the Bordezac reference sample by using

PyMCA software to quantify each chemical element. We calculated the concentration of each element from the areas under the peaks by applying a configuration file that enabled us to take into account the following device parameters:

- Mathematical spectrum fit parameters (MCA Hypermet, Poisson's law for statistical weighting, 60 iterations applied between channels 130 and 1500) (Solé et al. 2007).
- ELIO system parameters: X-ray tube, 1-mm colimator, X-ray detector with SDD capsule, distance control by camera and laser beam: 1.4 cm (Calligaro et al. 2018)
- Standard parameters for the standard matrices (density 1 g/cm^3, 1-cm thick, percent composition by mass for BX-N: SiO_2 7.4; Al_2O_3 54.21; Fe_2O_3 23.17; TiO_2 2.37; H_20 11.48 and for DR-N: SiO_2 52.85; Al_2O_3 17.52; Fe_2O_3 9.7; MgO 4.4; CaO 7.05; Na_2O 2.99).

By processing the pXRF spectra in this way, we were able to quantify major, minor and trace elements. Major elements, defined as those whose oxides accounted for more than 5% of the total mass, were Al, Si and Fe. Minor elements, defined as those whose oxides accounted for between 0.005% and 5% of the total mass, were Na, Mg, P, K, Ca and Mn. Trace elements occurred in quantities of between 1 ppm and around several hundred ppm, which is below our pXRF spectrometer's detection limit.

4. Results – discussion

4.1 In-situ pXRF analysis of limestone and pictorial matter on the cave walls

We were able to conduct pXRF analyses of all 27 of the graphic entities on the decorated panels in the *Grotte aux Points*: *points-paumes*, animal figures and abstract marks. In total, we analysed 43 points on the pictorial matter (2 or 3 points for each graphic entity) and 23 points on bare limestone adjacent to the pictorial matter (Table 1 and 1bis).

PLEASE INSERT TABLE.1 AND 1.bis HERE

We began by examining the spectra obtained on the bare walls. The PCA on the pXRF spectra of points outside the pictorial matter (23 points) revealed two chemically distinct types of matter within the environmental signal (Figure 4):

(i) The first component is calcium, which explains 65.7% of the variance. This component corresponds to the Urgonian limestone substrate, which is predominantly calcium carbonate ($CaCO_3$) associated with a cortege of minor and trace elements (Al, Si, S, K, Ti, V, Cr, Mn, Fe, Ni, Zn, Sr). This limestone also contains occasional marine fossils;

(ii) The second component is sulphur, which explains 21.1% of the variance. This component corresponds to the thin, off-white deposits that occur intermittently throughout the cave, both on the graphic entities and the bare rock (Fig 4). These deposits are predominately calcium sulphate and may be alteration products resulting from the dissolution and precipitation of iron sulphide (pyrite, FeS_2) in the limestone (Boulvain 2010).

The presence of Ti, V, Cr, Mn, Ni, Zn, As and, especially, Sr is due to the limestone's marine origin (Debrand-Passard 1984). Because these elements are present in the cave walls, their concentrations cannot be used as markers of the colouring matter unless they occur in much higher concentrations in the colouring matter than in the substrate.

PLEASE INSERT FIG.4 HERE

Analyses revealed strong similarities in the composition of the pictorial matter between all the panels (Figure 5). The largest peaks in the pictorial matter spectra correspond to iron, which is accompanied by a cortege of minor and trace elements (Ti, V, Cr, Mn, Ni, Zn, As, Sr). These are the same minor and trace elements as in the limestone. Apart from having a much higher iron content, the pictorial matter has a qualitatively similar composition to that of the limestone substrate.

PLEASE INSERT FIG.5 HERE

We performed a second PCA on the pXRF spectra of points on the bare walls and the pictorial matter (Figure 6).

i) PC1 is the limestone substrate, which explains 75.8% of the total variance.

ii) PC2 is the iron-rich matter, which explains 20.9% of the total variance.

Even if there is a tendency to rank the analysis points according to their iron composition (PC2: 20.9%), the PCA did not enable us to differentiate between analysis points on the bare rock and those on the pictorial matter.

PLEASE INSERT FIG.6 HERE

Because X-rays penetrate below the target surface, the volume analysed at each of our target points was approximately 1 mm^3. Thus, our analyses of pictorial matter were actually analyses of the pictorial matter plus the underlying Urgonian limestone substrate and, occasionally, calcium sulphate deposits. As there is currently no mathematical method available for subtracting the background composition (Gay, 2015), the chemical composition of the pictorial matter cannot be determined independently of the substrate or alteration phases, so we were unable to determine geochemical signatures for the pictorial matter in the Grotte aux Points.

4.2. Laboratory analyses of pigmented flakes

In order to validate our results, we used the same pXRF spectrometer to carry out laboratory analyses of flakes of rock bearing patches of pictorial matter. As for the in-situ analyses of the graphic entities, the spectra of these flakes of pigmented rock included an environmental signal (Al, Si, K, Ca, P, etc.) due to the limestone substrate and to clay minerals and alteration products that were deposited on the flakes when they fell onto the cave floor. Consequently, the laboratory analyses did not provide any more useful information about the pictorial matter than the in-situ analyses.

Hence, the main limiting factor in pXRF analyses of iron-based colouring matter is not the measurement environment (cave or laboratory), but the nature of the objects being analysed, as it is impossible to extract a meaningful chemical signal from colouring matter that is spread thinly but unevenly over a substrate and partly covered by alteration products.

4.3. Laboratory analyses of blocks of colouring matter

We also used pXRF to determine the geochemical signatures of blocks of colouring matter, in order to ascertain whether these signatures would substantiate our division of the blocks into lithological categories based on their petrographical characteristics. We carried out pXRF analyses of two points on each of 48 blocks of colouring matter (Table 2).

PLEASE INSERT TABLE 2 HERE

A PCA on the processed spectra (Matlab routine) revealed two components (Figure 7):

- PC1 (61.1 % of the total variance), defined by the environmental signal, comprised blocks whose surfaces were partly or entirely covered by calcite deposits (6 blocks, 1 point/block). In this case, the marker elements of the environmental signal were K, Ca and Ti, which occur both in the calcite deposits and in the sediment of the archaeological layer, which also contained markers of the surrounding rock.

- PC2 (20.9% of the total variance), defined by iron content, consisted of blocks with no, or only very minor, calcite deposits. However, this PCA did not reveal any significant differences in the compositions of the different types of colouring matter identified by visual/petrographical analysis.

PLEASE INSERT FIG.7 HERE

In order to reduce the number of PCA variables (4,096 channels) and to evaluate the possibility of distinguishing lithological groups on the basis of pXRF analyses, we performed a second PCA based only on the peak areas of elements in the spectra of blocks of colouring matter with no calcite crust.

For this PCA we introduced as variables just those chemical elements whose concentrations were within the instrument's detection limits and present as major or minor elements in ferruginous rocks: Al, Si, K, Ca, Ti. We chose these elements also because their relative proportions provide markers of the major rock types: sedimentary rocks, volcanic rocks, or products of continental weathering.

All the samples had very high and very variable iron contents, so we normalised the area under the peak for each chemical element, calculated using PyMCA software, with respect to the sample's iron content.

PLEASE INSERT FIG.8 HERE

Results of this second PCA of the spectra of blocks of colouring matter (Figure 8) were very similar to those of the previous PCA, even though we entered fewer variables and excluded samples with calcite crusts.

Although the first two components explained almost all of the variance—83.9% for PC1, defined by Ca and K; 12.3% for PC2, defined by Si and Ti—it is not possible to identify groups of raw materials corresponding to the lithologies described visually. Performing such a PCA does not seem to be appropriate because:

- There are no geological reference samples with which to compare our data, so we were unable to determine whether there are any real similarities or dissimilarities in the chemical compositions of the blocks of colouring material.

- All our analysis spectra probably included an environmental component, indicated by the presence of Ca and K, due to sediment coatings on the surface of the colouring matter. This is all the more likely because none of the archaeological remains were prepared prior to analysis.

- Uncertainty as to the reliability of the geochemical signatures obtained by quantifying our ferruginous matter analyses makes it difficult to ascertain the geological origins of this matter (no access to element detection limits).

These results highlight the impact of depositional and conservational factors on pXRF's ability to provide meaningful analyses of pictorial and colouring matter. The second part of our study explored pXRF's ability to identify and quantify the elements within a chemical signature. Our in-situ and laboratory analyses of samples from the *Grotte aux Points* showed the method's limitations when analysing unknown materials, but how do pXRF analyses compare with certified (ICP) and PIXE analyses of reference standards?

4.3 Standards

We assessed the ability of pXRF to provide robust quantitative geochemical analyses of ferruginous rocks, by carrying out pXRF and µPIXE analyses of the Bordezac, DR-N, and BX-N standards, and then comparing the results of these analyses with each other and with reference (ICP) analyses for the three standards. For all the samples and for each element, we calculated the differences between the quantities given by pXRF and by the reference analyses, and then performed similar calculations for the µPIXE and reference analyses. In all cases, there were large differences between the contactless methods and the reference analyses (Tables 3 and 3bis).

PLEASE INSERT TABLE 3 AND 3bis HERE

As neither pXRF nor µPIXE provided absolute values that can be used to directly determine chemical signatures, we compared the ratios between iron and other elements obtained using each method for each sample, in order to identify iron-related elements (Figure 9).

PLEASE INSERT FIG.9 HERE

Taking all the elements together (major, minor and trace), the pXRF analyses did not produce the same ratios as the ICP/certified values, with correlation coefficients ranging from 0.1 to 0.5 (Figure 9a). Nevertheless, because detection limits for trace elements are much higher than those for major and minor elements, the weight of the major and minor elements when plotted as graphs can create false correlations. When we considered major elements on their own, the ratios between them and iron were similar across analysis methods, with correlation coefficients of around 0.99 for all three standards (Figure 9b). However, this was not the case for the ratios between trace elements and iron, for which the pXRF-ICP

correlation coefficients were between 0.1 and 0.5 (Figure 9c). This is probably due to pXRF's quantification limits for these elements. In order to understand this phenomenon better, we plotted similar graphs for the results of the µPIXE analysis (Figure 9).

The µPIXE analyses differed substantially from the reference analyses. Considering all the elements together, correlation coefficients between the µPIXE and ICP element-iron ratios were around 0.90 for BX-N and Bordezac, which have relatively high iron contents, but close to 0 for DR-N, which has a low iron content (Figure 9d). This was also the case when we examined major and trace elements separately (Figure 9e and 9f).

The discrepancies between the ICP and PIXE element-iron ratios for DR-N can be attributed mostly to the fact that the treatment parameters in the configuration file we used for our analyses were adapted to iron-rich matrices and therefore not appropriate for DR-N's relatively low-iron matrix. This shows the importance of ensuring data processing tools are suited to the composition of the sample being analysed, notably its iron content.

Hence, different theoretical spectrum configuration files have to be used for matrices with different compositions, as models have to take into account the physical effects produced by certain elements, especially heavy elements such as iron. Consequently, the same parameters cannot be applied to DR-N (9.1% Fe_2O_3) and to BX-N and Bordezac (23.14% and 74.79% Fe_2O_3, respectively).

5. Conclusion

The present study examined the capabilities of current pXRF spectrometry techniques for analysing rock art. We did this by carrying out in-situ and laboratory analyses of a variety of objects and materials from the *Grotte aux Points* in southeast France, and by comparing pXRF analyses of reference samples with PIXE and ICP analyses of the same samples. Whether analysing decorated panels, flakes of pigmented rock or blocks of colouring matter, our results show it is essential to have a thorough understanding of the materials being analysed in order to decipher the information contained within fluorescence spectra.

Consequently, given the high detection limits of the elements typically present in ferruginous rocks and minerals (Calligaro et al. 2018; Shackeley 2010), it is not currently possible to use pXRF to precisely quantify and compare the chemical compositions of pictorial matter and blocks of colouring matter. In addition, our pXRF analyses did not allow us to assign a distinct chemical signature to the different lithologies of cohesive colouring matter identified on the basis of their morphological and petrological characteristics.

Our results suggest that carrying out systematic pXRF surveys of rock art prior to sampling is not worth the time and expense, or the risk to both the rock art and the equipment (due to manoeuvring the equipment in confined spaces). Although pXRF can provide information about the alteration phenomena affecting a cave's walls (presence of calcium sulphate), in-situ pXRF analyses do not provide more information than other contactless analysis methods, such as visual inspection using a binocular magnifier or macro photographs. Hence, a more appropriate approach would be to micro-sample the art following a detailed visual examination to choose the most suitable sampling points, taking into account the nature of the pictorial matter and the effects of alteration processes.

Acknowledgments
We would like to thank the ASTRE laboratory (USMB) and the Cité de la Préhistoire Grand Site de l'Aven d'Orgnac: funding provided by DRAC Occitanie and DRAC AURA (Pigmentothèque). We would also like to thank Claire Pacheco and her colleagues at C2RMF, Quentin Lemasson and Laurent Pichon, for providing access to AGLAE and technical support, the C2RMF – AGLAE laboratory, and SARM for the ICP analysis: funding provided by the AAP Mascara USMB 2018. Finally, we would like to thank the anonymous reviewers whose comments helped improve the draft manuscript.

Bibliography

Baffier, D., Feruglio, V. 1998**.** Premières observations sur deux nappes de ponctuations de la grotte Chauvet (Vallon-Pont-d'Arc, Ardèche, France). International Newsletter on Rock Art 21, 1–4.

Beck, L., Lebon, M., Pichon, L., Menu, M., Chiotti, L., Nespoulet, R., Paillet, P., 2011. PIXE characterisation of prehistoric pigments from Abri Pataud (Dordogne, France). X-Ray Spectrometry 40, 219–223. https://doi.org/10.1002/xrs.1321

Beck, L., Rousselière, H., Castaing, J., Duran, A., Lebon, M., Lahlil, S., Plassard, F. 2012. Analyse in situ des dessins préhistoriques de la grotte de Rouffignac par fluorescence X et diffraction X portable. ArcheoSciences. Revue d'archéométrie 36:139–152.

Beck, L., Lebon, M., Lahlil, S., Grégoire, S., Odin, G.P., Rousselière, H., Castaing, J., Duran, A., Vignaud, C., Reiche, I., Lambert, E., Salomon, H., Genty, D., Chiotti, L., Nespoulet, R., Lassard, F., Menu, M. 2014**.** Analyse non-destructive des pigments préhistoriques: de la grotte au laboratoire, Paleo ANR Madapca: 63-74

Boccaccio, G. 2018. Résultats préliminaires de l'étude de la série lithique de la grotte aux Points: typologie et technologie. Karstologia n°72: 37–44

Boulvain F., 2010. Pétrologie sédimentaire. Des roches aux processus, Technosup, ellipses, 259.

Brunel, E., Chauvet, J.M., Hillaire, C. 2018. La grotte aux Points d'Aiguèze: récits de découverte d'une ornementation pariétale. Karstologia n°72: 13–14

Brunel, E., Chailloux, D., Chauvet, J.-M., Hillaire, C., Raimbault, M., Renda, M., Terres, S. 2008. La Grotte aux Points (commune d'Aiguèze, Gard). Ardèche Archéologie, 25: 23-28

Calligaro, T., Castelle, M., Lebon, M., Mauran, G. 2019. Analyse par fluorescence des rayons X portable. In: Instrumentation portable : quels enjeux pour l'archéométrie ? C.

Benech, N. Cantin, M.A. Languille, A. Mazuy, L. Robinet, A. Zazzo. Editions Archives Contemporaines, septembre 2019

Chalmin, E., Menu, M., and Vignaud, C. 2003. Analysis of rock art painting and technology of Palaeolithic painters. Measurement Science and Technology, 14 (9), 1590.
Chalmin, E., Menu, M., Pomiès, M.-P., Vignaud, C., Aujoulat, N., and Geneste, J.-M. 2004. Les blasons de Lascaux. L'anthropologie, 108 (5), 571-92.

Chanteraud, C., Chalmin, E., Salomon, H., Hoerlé, S., Monney, J. 2019. Relation entre les matières colorantes issues des fouilles et des parois ornées. Méthodologie et première perspective comparative à la Grotte aux Points (Aiguèze, Gard, France). Karstologia n°73: 1 – 12

Chiotti, L., Nespoulet, R., Henry-Gambier, D., Vercoutere, C., Crépin, L., Lebon, M., Beck, L., Müller, C., Reiche, I. 2014 Un comportement funéraire original au Gravettien Final. Bilan des analyses et études 2005-2011 de la couche 2 de l'abri Pataud (Les Eyzies-de-Tayac, Dordogne). In: Paillet P (ed) Les arts de la Préhistoire: micro-analyses, mises en contexte et conservation, actes du colloque MADAPCA, 16-18 novembre 2011. Paléo, numéro spécial, pp 183–93

Eiselt, BS, Popelka-Filcoff, RS, Darling, JA, Glascock, MD. 2011. Hematite sources and archaeological ochres from Hohokam and O'odham sites in central Arizona: an experiment in type identification and characterization. Journal of Archaeological Science, 38(11), 3019-3028

d'Errico, F., Dayet Bouillot, L., García-Diez, M.,Pitarch Martí, A., Garrido Pimentel, D., Zilhão, J. 2016. The technology of the earliest European cave paintings: El Castillo Cave, Spain. Journal of Archaeological Science 70, 48–65.

Dayet, L., Le Bourdonnec, F., Daniel, F., Porraz, G., Texier, P., 2016. Ochre provenance and procurement strategies during the middle stone age at Diepkloof Rock Shelter, South Africa. Archaeometry 58, 807–829.

Dayet, L., Faivre, J.-Ph., Le Bourdonnec,F.-X., Discamps, E., Royer, A., Claud, E., Lahaye, C., Tartar, E., Cantin, N., Queffelec, A., Gravina, B., d'Errico, F., Turq, A. 2019. Manganese and iron oxide use at Combe-Grenal (Dordogne, France): A proxy for cultural change in Neanderthal communities. Journal of Archaeological Science: Reports 25: 239-256.

Debrand-Passard, S. 1984. Synthèse géologique du Sud-Est de la France. Editions du Bureau de recherches géologiques et minières, Service géologique national.

Defrasne, C., Chalmin, E., Bellot-Gurlet, L., Thirault, E., André, G. 2019. From archeological layers to schematic rock art? Integrated study of the Neolithic pigments and pigmented

rocks at the Rocher du Château (Western Alps, Savoie, France). *Archaeological and Anthropological Sciences* 11, n^{o} 11: 6065-91.

Gay, M., Plassard, F., Muller, K., Reiche, I. 2020 Relative chronology of Palaeolithic drawings of the Great Ceiling, Rouffignac cave, by chemical, stylistic and superimposition studies. Journal of Archaeological Science Rep. 29

Gay, M., Muller, K., Plassard, F., Cleyet-Merle, J.-J., Arias, P., Ontañón, R., Reiche, I. 2016. Efficient quantification procedures for data evaluation of portable X-ray fluorescence – Potential improvements for Palaeolithic cave art knowledge. J. Archaeolog. Sci.: Rep. 10: 878–886

Gay, M. (2015). Développement de nouvelles procédures quantitatives pour une meilleure compréhension des pigments et des parois des grottes ornées préhistoriques, PhD Thesis, Université Pierre et Marie Curie-Paris VI.

Goemaere, É., Salomon, H., Billard, C., Querré, G., Mathis, F., Golitko, M., Dubrulle-Brunaud, C., Savary, X., Dreesen, R., 2016. Les hématites oolithiques du Néolithique ancien et du Mésolithique de Basse-Normandie (France): caractérisation physico-chimique et recherche des. Anthropologica et Praehistorica 125, 89–119.

Henry-Gambier, D., 2008. Comportement des populations d'Europe au Gravettien : pratiques funéraires et interprétations. PALEO. Revue d'archéologie préhistorique 399–438.

Huntley, J., Aubert, M., Ross, J., Brand, H., Morwood, M.J. 2015. One colour (at least) two minerals: a study of mulberry rock art pigment and a mulberry pigment 'quarry' from the Kimberley, northern Australia. Archaeometry, 57 (1): 77–99

Huntley, J. and Galamban, D. 2016. The material scientific investigation of Rock Art : Contributions from non-invasive X-ray techniques. In Palaeoart and Materiality
The Scientific Study of Rock Art edited by Robert G. Bednarik, Danae Fiore, Mara Basile, Giriraj Kumar and Tang Huisheng. Archeopress Archaeology. 41-58

Huntley, J. 201). Taphonomy and paint recipes. Australian Archaeology, Vol.75: 78-94

Jaillet, S., Monney, J. 2018. Analyse 3D des volumes et des remplissages souterrains de la grotte aux Points au temps des fréquentations paléolithiques (Aiguèze, Gard). Karstologia n°72: 27–36

Lebon, M., Pichon, L., Beck, L., 2018. Enhanced identification of trace element fingerprint of prehistoric pigments by PIXE mapping. Nuclear Instruments and Methods in Physics Research Section B: Beam Interactions with Materials and Atoms 417, 91–95. https://doi.org/10.1016/j.nimb.2017.10.010

Lebon, M., Gallet, X., Bondetti, M., Pont, S., Mauran, G., Walter, P., Bellot-Gurlet, L., Puaud, S., Zazzo, A., Forestier, H., Auetrakulvit, P., Zeitoun, V. 2019. Characterization of painting pigments and ochres associated with the Hoabinhian archaeological context at the rock-shelter site of Doi Pha Kan (Thailand). Journal of Archaeological Science: Reports 26, 101855.

Leroi-Gourhan, A., Allain, J., 1979. Lascaux inconnu. CNRS.

Liritzis,I., Zacharias, N. 2011. Portable XRF of archaeological artifacts: current research, potentials and limitations. In: Shackley, M.S. (Ed.), X-ray Fluorescence Spectrometry (XRF) in Geoarchaeology. Springer, New York, pp. 109e142.

Mathis, F., Bodu, P., Dubreuil, O., Salomon, H. 2014. PIXE identification of the provenance of ferruginous rocks used by Neanderthals. Nuclear Instruments and Methods in Physics Research Section B: Beam Interactions with Materials and Atoms, vol. 331: 275–279

Mauran, G., Lebon, M., Détroit, F., Caron, B., Nankela, A., Pleurdeau, D., Bahain, J.-J. 2019. First in situ pXRF analyses of rock paintings in Erongo, Namibia: results, current limits and prospects. Archaeological and anthropological Sciences.

Monney, J. 2018a. La grotte aux Points d'Aiguèze, petite sœur de la grotte Chauvet, et les recherches menées dans le cadre du projet « Datation Grottes Ornées ». Karstologia, n°72: 1-12

Monney, J. 2018b. L'art pariétal paléolithique de la Grotte aux Points d'Aiguèze: Définition d'un dispositif pariétal singulier et discussion de ses implications. Karstologia, n°72: 45-57

Moyo, S., Mphuthi, D., Cukrowska, E., Henshilwood, C.S., Niekerk, K. van, Chimuka, L., 2016. Blombos Cave: Middle Stone Age ochre differentiation through FTIR, ICP OES, ED XRF and XRD. Quat. Int. 404, 20–29.
https://doi.org/10.1016/j.quaint.2015.09.041

Nuevo, M.J., Sánchez, A.M., Oliveira, C., Oliveira, J. de (2012). In situ energy dispersive X-ray fluorescence analysis of rock art pigments from the 'Abrigo dos Gaivões' and 'Igreja dos Mouros' caves (Portugal). X-Ray Spectrometry 41, 1–5.

Olivares M, Castro K, Corchón MS, Gárate D, Murelaga X, Sarmiento A, Etxebarria N 2013 Non-invasive portable instrumentation to study Paleolithic rock paintings: the case of La Peña Cave in San Roman de Candamo (Asturias, Spain). J Archeol Sci 40:1354–1360

Paillet, P. 2014. Introduction. Le programme ANR MADAPCA:" Micro-analyses et datations de l'art préhistorique dans son contexte archéologique", Paleo ANR Madapca: 13–16

Panchuk, V., Yaroshenko, I., Legin, A., Semenov, V., Kirsanov, D. 2018. Application of chemometric methods to XRF-data–A tutorial review. Analytica Chimica Acta 1040, 19–32.

Pearson, K. 1901. On lines and planes of closest fit to systems of points in space. Philos. Mag. 2: 559–572

Pichon, L., Beck, L., Walter, P., Moignard, B., Guillou, T. 2010. A new mapping acquisition and processing system for simultaneous PIXE-RBS analysis with external beam. Nuclear Instruments and Methods in Physics Research Section B: Beam Interactions with Materials and Atoms, 268 (11): 2028–2033

Pitarch A, Ruiz JF, Fernandez-Ortiz S, Hernanz A, Maguregui M, Madariaga JM. 2014. In situ characterization by Raman and X-ray fluorescence spectroscopy of post-Paleolithic blackish pictographs exposed to the open air in Los Chaparros shelter (Albalate del Arzobispo, Teruel, Spain). Anal. Methods. 6: 6641–6650.

Pradeau, J.-V., Binder, D., Verati, C., Lardeaux, J.-M., Dubernet, S., Lefrais, Y., Regert, M. 2016. Procurement strategies of Neolithic colouring materials: Territoriality and networks from 6th to 5th millennia in North-Western Mediterranean. J. Archaeolog. Sci. 71: 10–23

Pradeau, J.-V. 2015. Les Matières Colorantes au Sein des Systèmes Techniques et Symboliques au Néolithique (VIe et Ve millénaires BC) dans l'arc liguro-provençal. Thèse de doctorat, Université Nice Sophia Antipolis.

Popelka-Filcoff, R.S., Robertson, J.D., Glascock, M.D. et al. 200). Trace element characterization of ochre from geological sources. J Radioanal Nucl Chem 272, 17–27. https://doi.org/10.1007/s10967-006-6836-x

Rifkin, R.F., Prinsloo, L.C., Dayet, L., Haaland, M.M., Henshilwood, C.S., Diz, E.L., Moyo, S., Vogelsang, R., Kambombo, F. 2016. Characterising pigments on 30000-year-old portable art from Apollo 11 Cave, Karas Region, southern Namibia Journal of Archaeological Science: Reports. 5: 336-347

Roldán, C., Villaverde, V., Ródenas, I., Novelli, F., Murcia, S. 2013. Preliminary analysis of Palaeolithic black pigments in plaquettes from the Parpalló cave (Gandía, Spain) carried out by means of non-destructive techniques. Journal of Archaeological Science 40(1), 744-754.

Roldán C, Murcia S, Ferrero J, Villaverde V, López E, Domingo I, et al. 2010 Application of field portable EDXRF spectrometry to analysis of pigments of Levantine rock art. X-Ray Spectrometry. 39: 243–250.

Rosso, D.E., Marti, A.P., d'Errico, F., 2016. Middle Stone Age ochre processing and behavioural complexity in the horn of Africa: evidence from porc-epic Cave, Dire Dawa, Ethiopia. PloS one 11.

Salomon, H., Chalmin, E. 2019. Constitution d'une « Pigmentothèque » : un outil pour comprendre l'approvisionnement en matériaux colorants durant la Préhistoire. [Rapport de recherche] Service Régional de l'Archéologie Auvergne-Rhône-Alpes

Salomon, H. 2018. L'industrie des matières colorantes durant le Solutréen, in: Les Solutréens, Civilisations et Cultures. Arles, pp. 141–155

Salomon, H., Vignaud, C., Coquinot, Y., Beck, L., Stringer, C., Strivay, D., D'Errico, F. 2012. Selection and heating of colouring materials in the Mousterian level of Es-Skhul (c. 100,000 years BP, Mount Carmel, Israel). Archaeometry 54: 698–722

Savitzky, A., Golay, M.J.E. 1964. Smoothing and Differentiation of Data by Simplified Least Squares Procedures. Anal. Chem. 36: 1627–1639

Sepúlveda M, Gutierrez S, Carcamo J, Oyadener A, Valenzuela D, Monti I, Santoro CM. 2015 In situ X-ray fluorescence analysis of rock art paintings along the coast and valleys of the Atacama desert, northern Chile. Journal of the Chilean Chemical Society 60(1): 2822–2826.

Shackley, M.S. (Ed.), 2010. X-Ray Fluorescence Spectrometry in Geoarchaeology. Springer-Verlag GmbH.

Shackley, M.S. 2011. An introduction to X-ray fluorescence (XRF) analysis in archaeology. In M.S. Shackley (Ed.), X-ray fluorescence spectrometry (XRF) in geoarchaeology. New York: Springer. 7-44

Shackley, M.S., 2012. Portable X-ray fluorescence spectrometry (pXRF): the good, the bad, and the ugly. Archaeology Southwest Magazine 26, 1–8.

Shackley, M.S., 2018. X-Ray Fluorescence Spectrometry (XRF). The Encyclopedia of Archaeological Sciences 1–5.

Speakman, R.J., Shackley, M.S., 2013. Silo science and portable XRF in archaeology: a response to Frahm. Journal of Archaeological Science 40, 1435–1443.

Solé, V.A., Papillon, E., Cotte, M., Walter, P., Susini, J. 2007. A multiplatform code for the analysis of energy-dispersive X-ray fluorescence spectra. Spectrochimica Acta Part B: Atomic Spectroscopy, 62(1): 63 – 68

Velliky, E.C., Barbieri, A., Porr, M., Conard, N.J., MacDonald, B.L., 2019. A preliminary study on ochre sources in Southwestern Germany and its potential for ochre provenance during the Upper Paleolithic. Journal of Archaeological Science: Reports 27, 101977.

Young, T., 2000. The Paviland ochres: characterisation and sourcing. Paviland Cave and the 'Red Lady'. A definitive report, Wasp for SCARA: England 205–225.

Data citation

Chanteraud, C., Chalmin, E., Salomon, H., 2019. pixe_rich_iron_standards_dataset. https://doi.org/10.6084/m9.figshare.9798431.v2

Chanteraud, C., Jacq, K., 2019. matlab_script_pXRFdata. https://doi.org/10.6084/m9.figshare.9791474.v1

Chanteraud, C., Lebon, M., Chalmin, E., Monney, J., 2019. pXRF_standard_cave_dataset. doi.org/10.6084/m9.figshare.9791432.v1

Chanteraud, C., Lebon, M., Chalmin, E., Salomon, H., 2019. pXRF_standard_laboratory_dataset. doi.org/10.6084/m9.figshare.9791462.v2

Chanteraud, C., Lebon, M., Chalmin, E., Monney, J., 2019. pXRF_november_2017_grotte_aux_points_campain_data.doi.org/10.6084/m9.figshare.9791405.v1

Chanteraud, C., Lebon, M., Chalmin, E., Monney, J., 2019. pXRF_april_2017_grotte_aux_points_campain_data.doi.org/10.6084/m9.figshare.9791210.v1

Figure captions

Graphical abstract: Schematic overview of the approach used in our study

Figure 1: Lithologies of the blocks of colouring matter described in the text.

Figure 2: Morphologies of the pictorial matter on the cave walls and on flakes of rock: a) Red residue applied by tracing (coloured paste, block?) on the Ibex panel; b) Red residue near the pictorial matter on the Ibex panel; c) Patch of colouring matter on the Grands Signes panel, large area covered by a layer of colouring matter; d) Patch of colouring matter on flake s-eca-02.

Figure 3: Photographs of the Elio Xglab analysis system in the contactless analysis position: a) in the Galerie aux Points (PTS-14), b) in front of the Ibex panel (Cheval PTS-04) and c) in the hollow of the Niche aux Points (PTS-15).

Figure 4: A PCA of the spectra obtained from the bare walls showed that the relation between Ca and S was consistent with the presence of calcium sulphate. Component 1 (PC1) is the limestone signal, which explains 44.5% of the variance; component 2 (PC2) is the calcium sulphate signal, which explains 31.2% of the variance. The unusual shape of the Ca peak, which combines a co-variant and an anti-variant peak, highlights the presence of Ca in both mineral phases.

Figure 5: pXRF spectra for the pictorial matter analyses

Figure 6: PCA on the spectra obtained from the bare walls and from the colouring matter on the walls. Component 1 (PC1) is the limestone (Ca) signal, which explains 75.8% of the variance; component 2 (PC2) is the layer of colouring matter, which explains 20.9% of the variance. There is no clear distinction between analyses of the bare wall and of the layers of pictorial material.

Figure 7: PCA on the pXRF spectra obtained from blocks of colouring matter. Component 1 is the environmental signal and is characterised by peaks indicating the presence of K, Ca and Ti in calcite crusts, and of sediment on the surface of the colouring matter. S is present in a previously overlooked calcium sulphate alteration phase. Component 2 is iron, the colouring element in the blocks. Because iron is so predominant, it is not possible to detect elements associated with it. The PCA defined a tight cluster of blocks with high iron contents, whereas the other blocks are spread along a line defined by the environmental signal. The unusual shape of the Fe peak, which combines a co-variant and an anti-variant peak, highlights the presence of Fe in both mineral phases.

Figure 8: PCA on the pXRF normalised spectra obtained from blocks of colouring matter without calcite deposits. Component 1 is K and Ca. Component 2 is Si and Ti. The PCA

defined a tight cluster of blocks with a variety of lithologies (A, Av, and C) lying on the Ca signal line, whereas the other blocks are scattered across the plot.

Figure 9: Plots of the logarithms of element-iron ratios for (a) all elements, (b) major elements and (c) trace elements, measured by pXRF and ICP (certified or not) for the DR-N, BX-N and Bordezac reference standards. For all three standards, we found correlations between the pXRF element-iron ratios and ICP element-iron ratios for the major, minor and trace elements. Plots of the logarithms of the element-iron ratios for (d) all elements, (e) major elements and (f) trace elements obtained by PIXE and by ICP for the DR-N, BX-N and Bordezac standards.

Table 1: Summary of the in-situ analyses of the bare walls and of the paintings and drawings, carried out at the Grotte aux Points in 2017

Table 1b: Summary of the in-situ analyses of the bare walls and of the paintings and drawings, carried out at the Grotte aux Points in 2017

Table 2: Summary of pXRF analyses of cohesive colouring matter with the number of measurements performed

Table 3: Concentration of major and minor elements (% oxide) of the international standards DR-N, BX-N, and the Bordezac reference given by the CRPG (certified values, line 1), obtained by pXRF in the cave (line 2), obtained by pXRF in the laboratory (line 3), obtained by PIXE analysis (line 4). The deviation (delta) from the expected value (certified value) is given for pXRF in the cave (line 5), for pXRF in the laboratory (line 6) and for PIXED (line 7).

Table 3bis: Concentration of trace elements (ppm) of the international standards DR-N, BX-N, and the Bordezac reference given by the CRPG (certified values, line 1), obtained by pXRF in the cave (line 2), obtained by pXRF in the laboratory (line 3), obtained by PIXE analysis (line 4). The deviation (delta) from the expected value (certified value) is given for pXRF in the cave (line 5), for pXRF in the laboratory (line 6) and for PIXED (line 7).

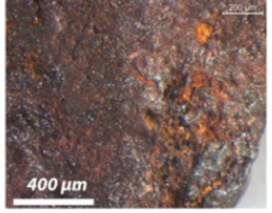

Lithology A

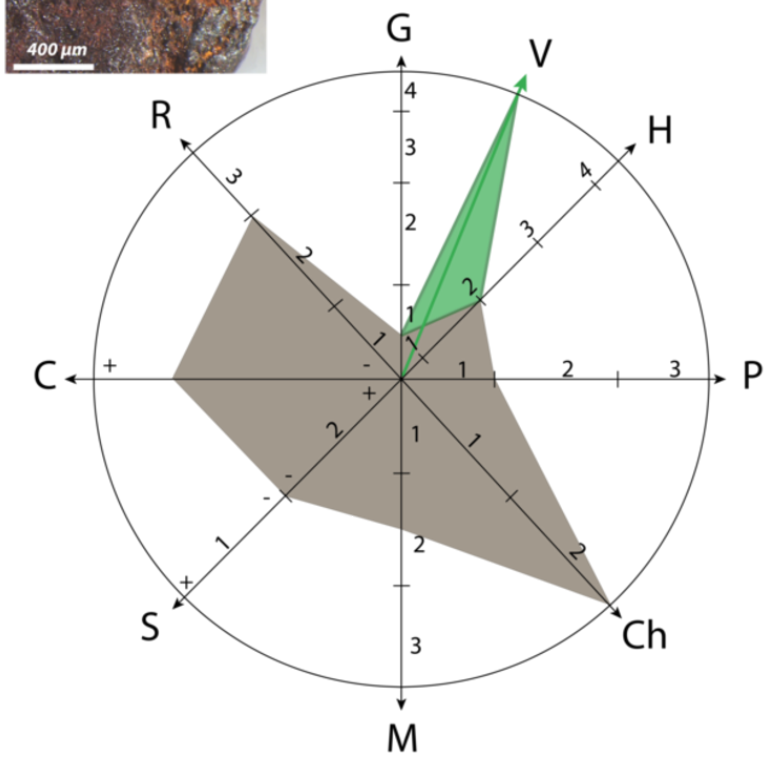

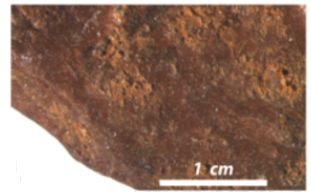

Lithology B

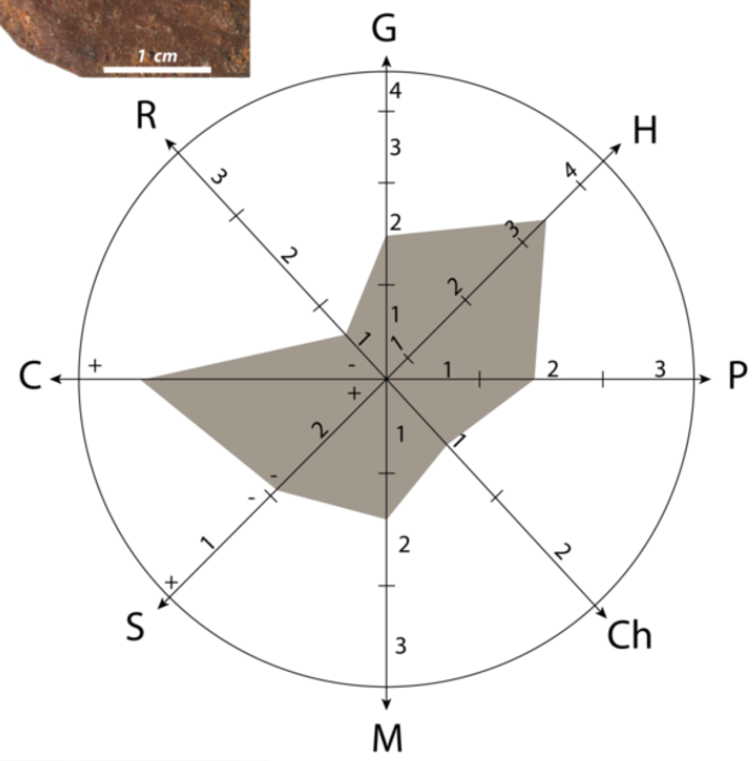

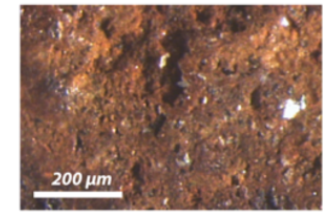

Lithology C

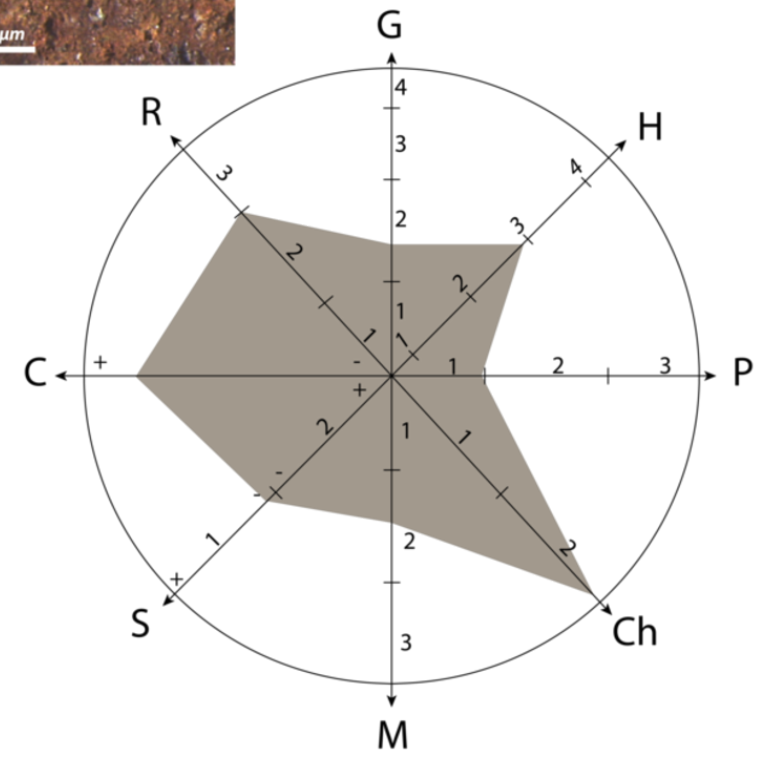

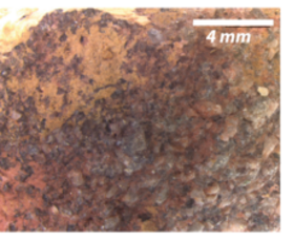

Lithology D

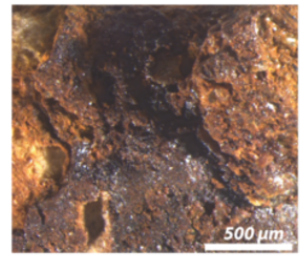

Lithology E

Legend

G: *Granulometry of stone explain with geological classification : from silt to sandstone*
1= clay; 2 = silt; 3 = thin sandstone; 4 = coarse sandstone

V *: Presence of green inclusions*

H: *Hardness based on theorical scale from*
1 = soft to 4 = hard

P: *Pore size explain with scale*
1 = micro; 2 = macro; 3 = mega

Ch: *Colouring mineral of the stone 1= goethite; 2 = hematite*

M : *Morphology of the cristal of iron oxy(hydro)xyde*
1=cubic; 2=tabular; 3=needle

S: *Surface quality 1= smooth ; 2 = angular*

C: *Cohesion of the rock : + = Cohesive ; - = loose*

R : *Lustre of the rock : 1 = matt; 2 = greasy; 3= metalic*

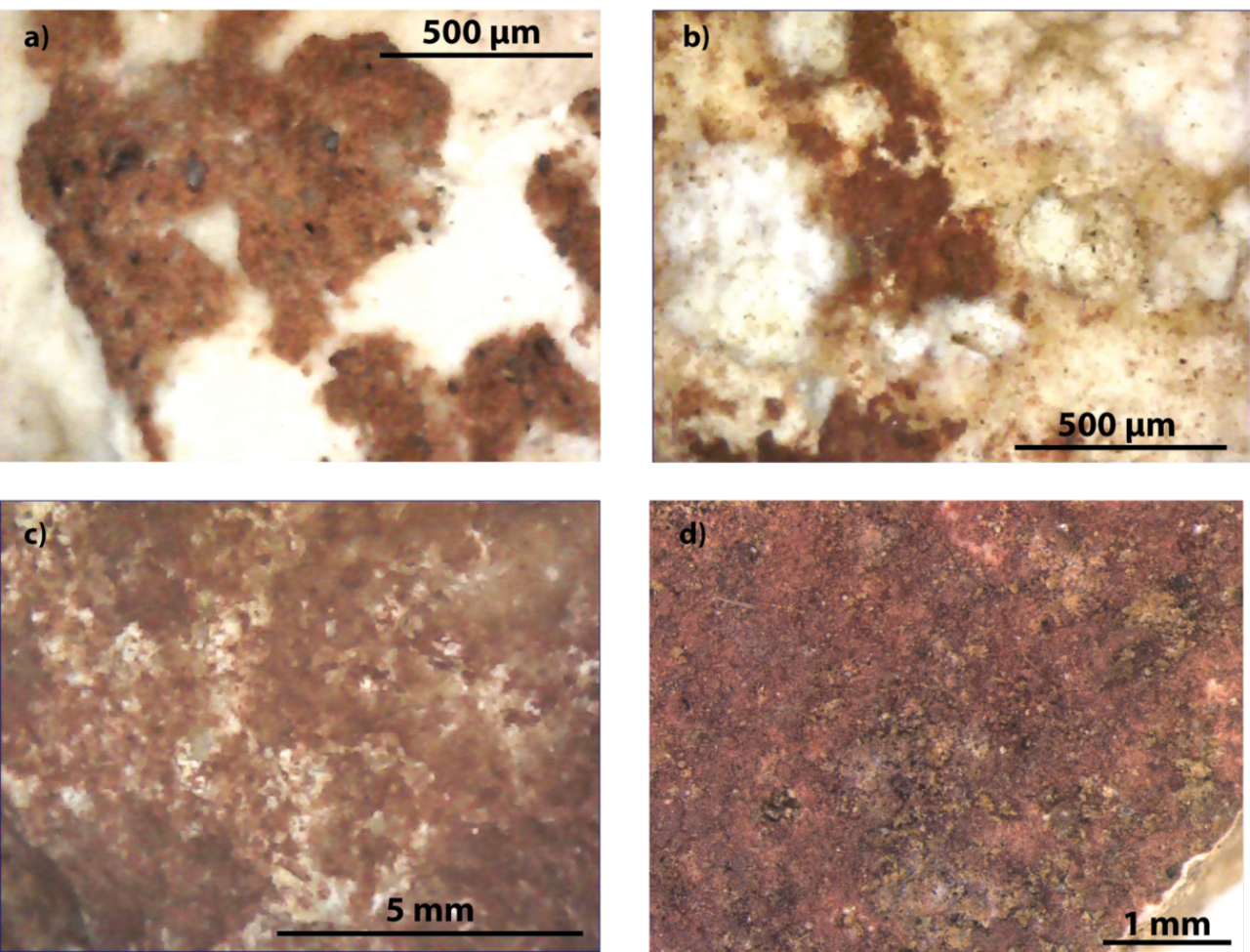
a)
500 µm
b)
500 µm
c)
5 mm
d)
1 mm


a)


b)


c)

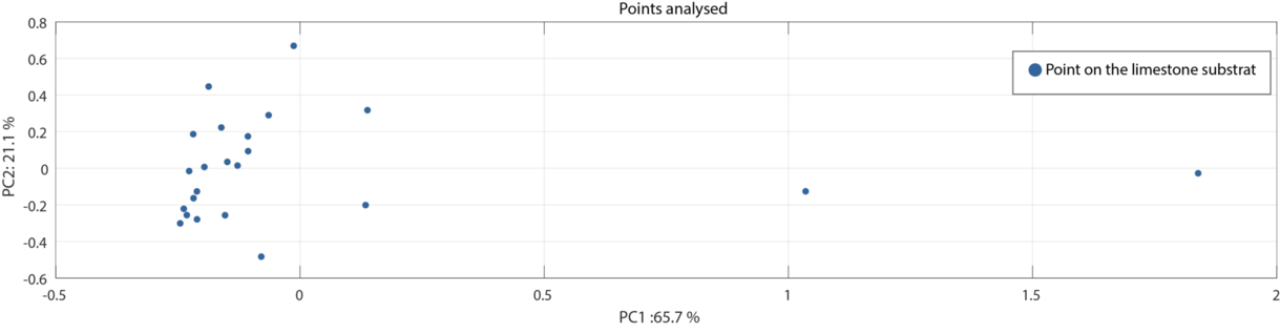
Points analysed
Point on the limestone substrat
PC2: 21.1 %
PC1 :65.7 %
0.8
0.6
0.4
0.2
0
-0.2
-0.4
-0.6
-0.5
0
0.5
1
1.5
2

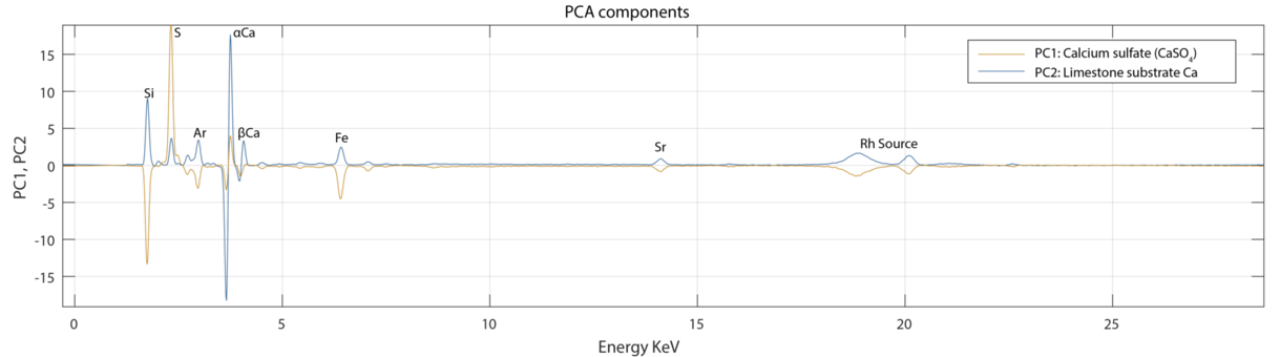
PCA components
PC1: Calcium sulfate ($CaSO_4$)
PC2: Limestone substrate Ca
PC1, PC2
Energy KeV
Si
S
αCa
Ar
βCa
Fe
Sr
Rh Source
15
10
5
0
-5
-10
-15
0
5
10
15
20
25

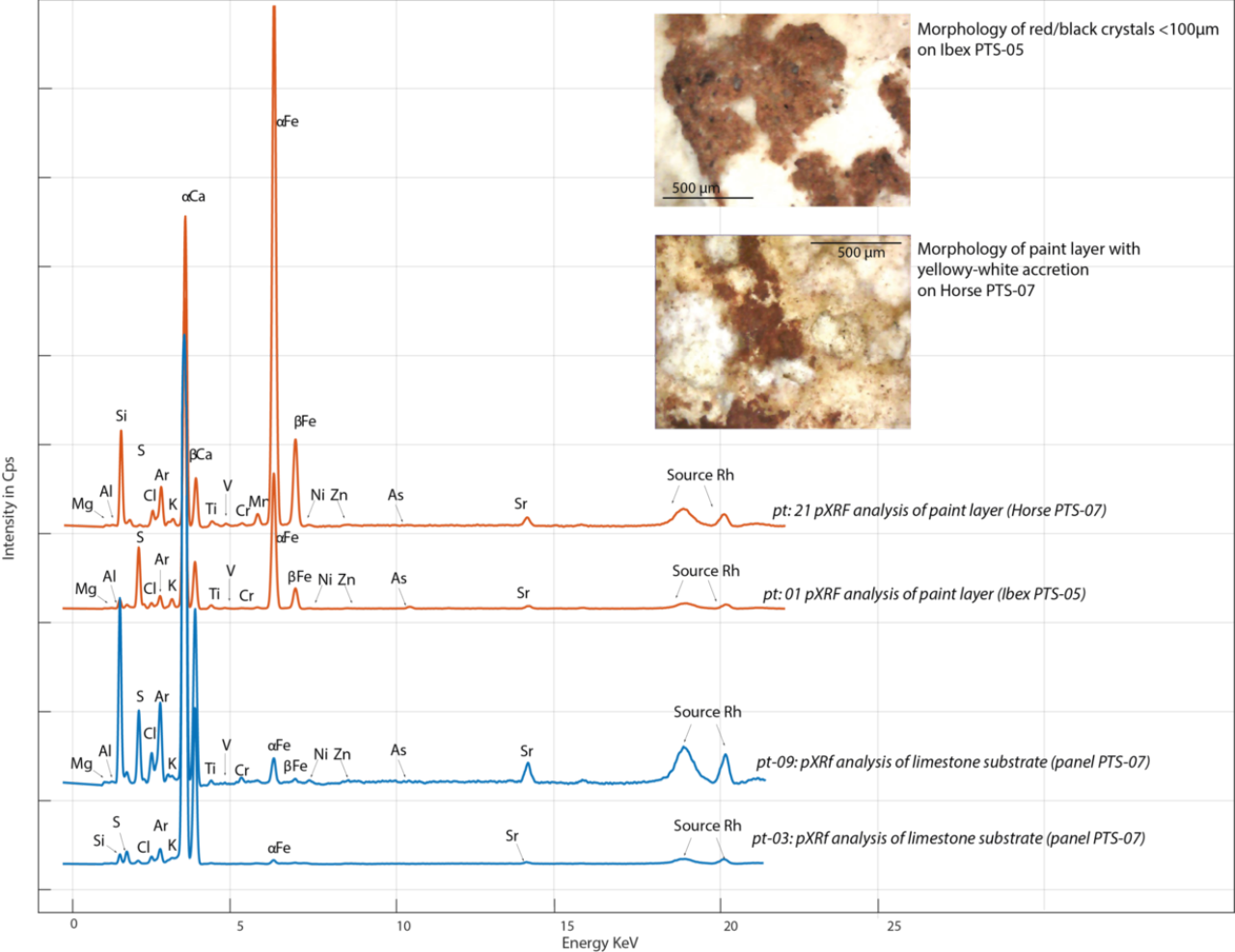
Morphology of red/black crystals <100µm on Ibex PTS-05
500 µm
Morphology of paint layer with yellowy-white accretion on Horse PTS-07
500 µm
Intensity in Cps
Energy KeV
0
5
10
15
20
25
αFe
αCa
βFe
βCa
Si
S
Ar
Cl
K
Mg
Al
Ti
V
Cr
Mn
Ni
Zn
As
Sr
Source Rh
pt: 21 pXRF analysis of paint layer (Horse PTS-07)
pt: 01 pXRF analysis of paint layer (Ibex PTS-05)
pt-09: pXRf analysis of limestone substrate (panel PTS-07)
pt-03: pXRf analysis of limestone substrate (panel PTS-07)

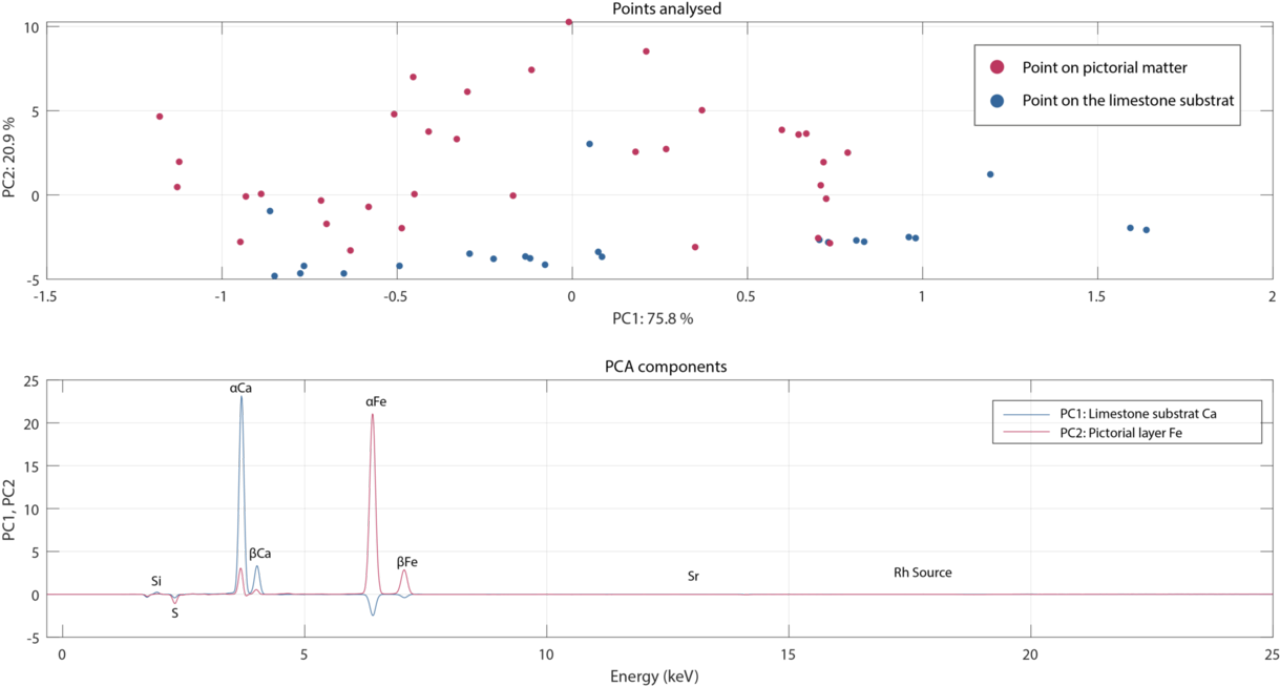
Points analysed
Point on pictorial matter
Point on the limestone substrat
PC2: 20.9 %
PC1: 75.8 %
PCA components
PC1: Limestone substrat Ca
PC2: Pictorial layer Fe
αCa
αFe
βCa
βFe
Si
S
Sr
Rh Source
PC1, PC2
Energy (keV)

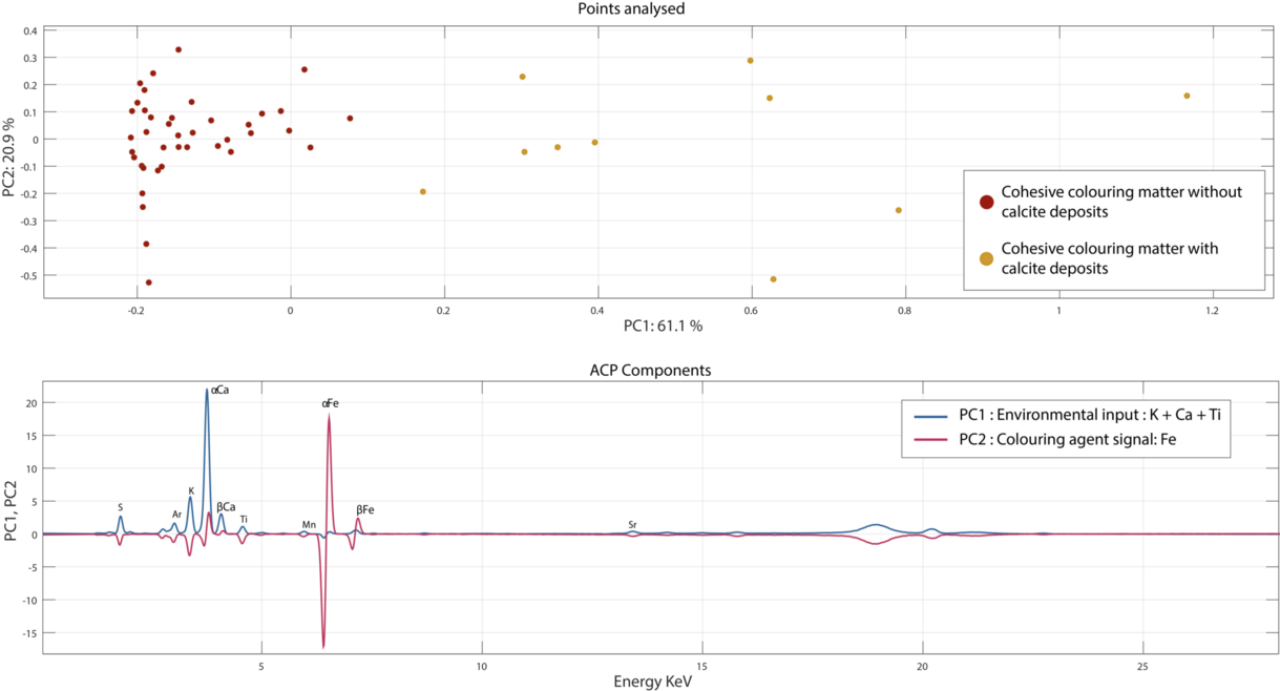
Points analysed
PC2: 20.9 %
PC1: 61.1 %
Cohesive colouring matter without calcite deposits
Cohesive colouring matter with calcite deposits
ACP Components
PC1, PC2
Energy KeV
PC1 : Environmental input : K + Ca + Ti
PC2 : Colouring agent signal: Fe
αCa
αFe
S
Ar
K
βCa
Ti
Mn
βFe
Sr

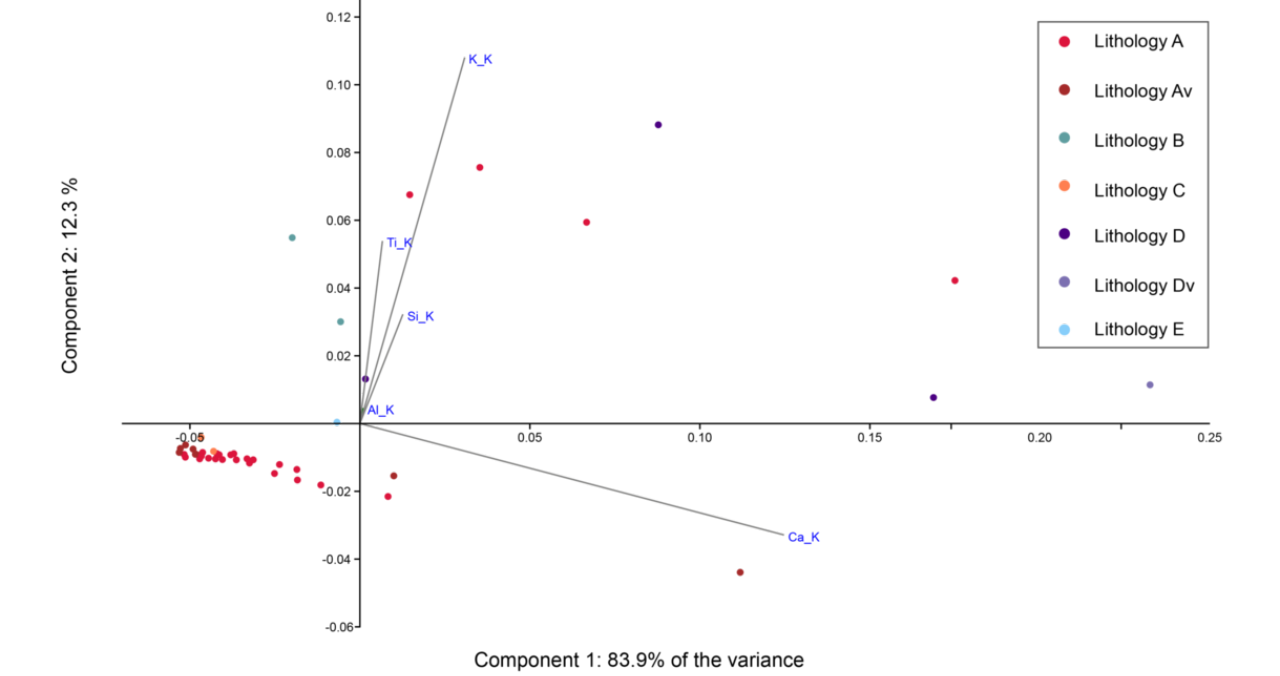
Component 2: 12.3 %
Component 1: 83.9% of the variance
K_K
Ti_K
Si_K
Al_K
Ca_K
Lithology A
Lithology Av
Lithology B
Lithology C
Lithology D
Lithology Dv
Lithology E

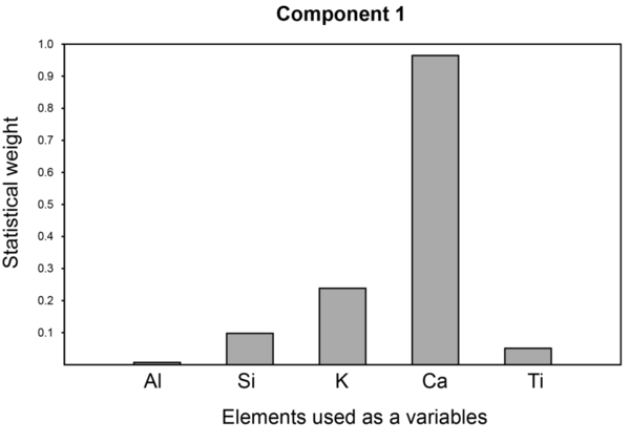
Component 1
Statistical weight
Al
Si
K
Ca
Ti
Elements used as a variables

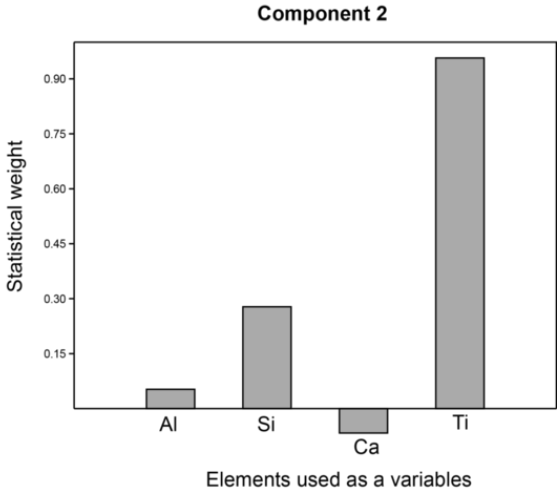
Component 2
Statistical weight
Al
Si
Ca
Ti
Elements used as a variables

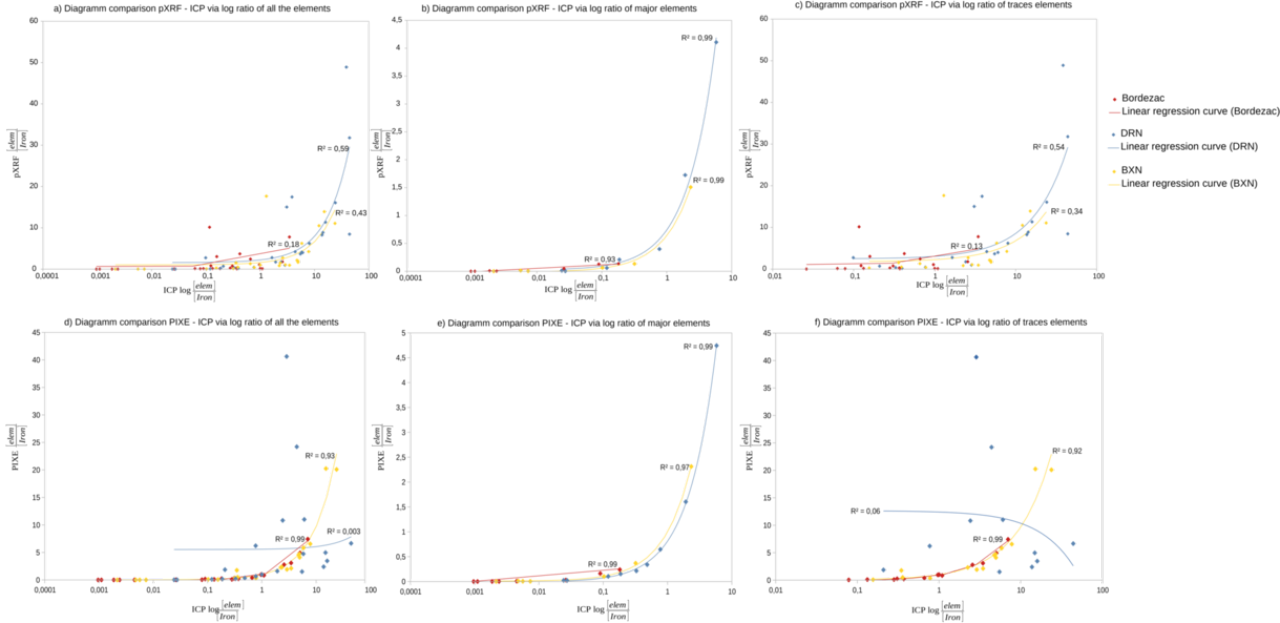
a) Diagramm comparison pXRF - ICP via log ratio of all the elements
b) Diagramm comparison pXRF - ICP via log ratio of major elements
c) Diagramm comparison pXRF - ICP via log ratio of traces elements
d) Diagramm comparison PIXE - ICP via log ratio of all the elements
e) Diagramm comparison PIXE - ICP via log ratio of major elements
f) Diagramm comparison PIXE - ICP via log ratio of traces elements
pXRF log (elem/Iron)
PIXE log (elem/Iron)
ICP log (elem/Iron)
R² = 0,59
R² = 0,43
R² = 0,18
R² = 0,99
R² = 0,99
R² = 0,93
R² = 0,54
R² = 0,34
R² = 0,13
R² = 0,93
R² = 0,99
R² = 0,003
R² = 0,99
R² = 0,97
R² = 0,99
R² = 0,06
R² = 0,99
R² = 0,92
Bordezac
Linear regression curve (Bordezac)
DRN
Linear regression curve (DRN)
BXN
Linear regression curve (BXN)

Pannel	Localization		Acquisition number	Nature	Description macro	
	Figure	zone			deposit	inclusion
Ibex+E3	PTS 05	Bottom of right outline	1	Pictorial matter	Red drawing with block?	Black
			2	Pictorial matter	Red drawing with block?	Black
			3	Bare wall	-	-
		Middle of left outline	4	Pictorial matter	Red drawing with block?	Black
			5	Bare wall	-	Localized black deposit
	PTS 04	Head	6	Pictorial matter	Red drawing with block ?	Black
			7	Bare wall	-	Localized black deposit
		Back	8	Pictorial matter	Red drawing with block?	-
			9	Bare wall		-
		Right foreleg	10	Pictorial matter	Red drawing with block?	Black
			11	Bare wall		-
	PTS 03	Red mark at the top	12	Pictorial matter	Red drawing with block?	Localized black deposit
		Centre red mark	13	Bare wall	-	Localized black deposit
		Black outline	14			
Galerie aux Points	PTS 14	Pointe paume 3	15	Pictorial matter	Red palm point	-
		Middle of the figure	16	Bare wall	-	-
		Pointe paume 1	17	Pictorial matter	Red palm point	-
	PTS 13	Bottom right	18	Pictorial matter	Red palm point	-
		Bottom right	19	Bare wall	-	-
Horse & Bison	PTS-07	Chin	20	Pictorial matter	Red drawing with block?	-
			21	Pictorial matter	Red drawing with block?	-
			22	Bare wall	-	-
	PTS-08	Back	23	Pictorial matter	Red drawing with block?	-
			24	Bare wall	-	-
Grands Signes	PTS-09	Top part	25	Pictorial matter	Colouring matter applied with palm	-
			26	Pictorial matter		-
			27	Bare wall	-	-
	PTS-10	Top part	28	Pictorial matter	Colouring matter applied with palm	-
			29	Pictorial matter		-
			30	Bare wall	-	-

cancelled point

Remains number	Lithology	Spectrum number	Environmental brand
16-15	A	2	unobservable
16-14	A	2	unobservable
16-03	A	2	unobservable
16-02	A	2	unobservable
16-08	C	2	unobservable
16-12	E	2	unobservable
16-10	A	2	unobservable
16-11	B	2	unobservable
16-06	A	2	unobservable
16-04	A	2	unobservable
16-07	A	2	unobservable
16-05	A	2	unobservable
16-09	Av	2	unobservable
15-03	A	2	unobservable
15-05	A	2	unobservable
15-11	A	2	unobservable
15-14	A	2	unobservable
15-12	D	2	unobservable
15-02	A	2	unobservable
15-16	A	2	unobservable
15-07	D	2	unobservable
15-17	A	2	unobservable
15-229	A	2	unobservable
15-13	A	2	unobservable
15-04	Av	2	unobservable
15-13	A	2	unobservable
15-09	D	2	unobservable
15-10	A	2	unobservable
15-01	C	2	unobservable
15-06	Av	2	unobservable
15-231	Dv	2	unobservable
14-201	A	2	calcite deposit
13-17	Av	2	unobservable
11-01	A	2	calcite deposit
14-206	A	2	calcite deposit
14-213	A	2	calcite deposit
14-212	Av	2	unobservable
13-10	Av	2	unobservable
13-18	A	2	unobservable
13-16	Av	2	unobservable
13-11	A	2	calcite deposit
13-07	Av	2	unobservable
13-08	A	2	unobservable
13-09	A	2	unobservable
13-15	A	2	unobservable
13-14	A	2	calcite deposit
15-08	B	2	unobservable

	Major elements %										Traces elements (ppm)																									
	Na2O	*MgO*	*Al2O3*	*SiO2*	*P2O5*	*K2O*	*CaO*	*TiO2*	*MnO*	*Fe2O3*	*S*	*Cl*	*Sc*	*V*	*Cr*	*Co*	*Ni*	*Cu*	*Zn*	*Ga*	*Ge*	*As*	*Rb*	*Sr*	*Y*	*Zr*	*Nb*	*Mo*	*In*	*Sb*	*Cs*	*Ba*	*La*	*Hf*	*W*	*Pb*
DRN						**DRN**																		**DRN**												
ref fiche	2.99	4.4	17.52	52.85	0.25	1.70	7.05	1.09	0.22	9.10	350	400	28	220	40	35	15	50	145	22	1.9	3	73	400	26	125	7	0.9	0.08	0.4	6.3	385	21.5	3.6	130	55
grotte	< L.D.	< L.D.	24.44	37.26	0.28	1.78	3.20	0.48	0.09	8.02	125	732	1	132	91	402	45	28	90	20	3	< L.D.	46	218	16	91	10	6	< L.D.	< L.D.	< L.D.	< L.D.	< L.D.	21	98	52
labo	< L.D.	< L.D.	14.67	34.93	0.02	1.78	3.39	0.51	0.10	8.50	416	72	128	137	36	149	24	31	96	15	6	3	53	270	8	70	4	23	< L.D.	< L.D.	< L.D.	< L.D.	< L.D.	1	75	34
pixe	3.87	4.69	19.29	54.80	0.27	1.47	5.91	0.86	0.20	8.41	390	376	-	190	< L.D.	-	13	26	117	14	3	< L.D.	63	343	25	51	8	< L.D.	-	< L.D.	-	631	< L.D.	-	90	48
BXN						**BXN**																		**BXN**												
ref fiche	0.04	0.11	54.21	7.4	0.13	0.05	0.17	2.37	0.05	23.14	-	-	60	350	280	30	180	18	80	67	1.1	115	3.6	110	114	550	52	8.3	0.3	8	0.4	30	355	15.2	9	135
grotte	< L.D.	< L.D.	38.57	3.87	0.23	0.05	0.09	1.37	0.04	20.80	125	175	112	230	229	698	92	18	30	25	1	30	10	41	40	181	23	1	< L.D.	< L.D.	< L.D.	< L.D.	< L.D.	11	17	129
labo	< L.D.	< L.D.	33.94	3.01	0.29	0.03	0.08	1.42	0.02	22.50	299	309	61	313	237	397	95	9	21	24	0	38	6	48	45	249	19	35	< L.D.	< L.D.	< L.D.	< L.D.	< L.D.	30	11	140
pixe	< L.D.	0.31	60.32	9.65	0.15	0.06	0.12	2.66	0.05	26.08	118	4	-	499	302	< L.D.	170	11	63	54	3	104	< L.D.	119	122	624	63	14	-	25	-	< L.D.	< L.D.	-	24	151
IF-G						***IF-G***																		***IF-G***												
ref fiche	0.032	1.89	0.15	41.2	0.063	0.012	1.55	0.014	0.042	53.98	350	400	28	220	40	35	15	50	145	22	1.9	3	73	400	26	125	7	0.9	0.08	0.4	6.3	385	21.5	3.6	130	55
grotte	< L.D.	< L.D.	5.64	28.72	0.15	0.01	0.96	0.075	0.017	34.89	97	210	5	1	181	1117	3	21	12	4	12	3	16	3	2	4	2	6	< L.D.	< L.D.	< L.D.	< L.D.	< L.D.	8	47	134
labo	< L.D.	< L.D.	1.97	34.41	0.32	< L.D.	1.02	0.08	0.00	38.81	182	1061	16	46	117	546	2	17	9	2	2	< L.D.	19	1	6	3	3	24	< L.D.	< L.D.	< L.D.	< L.D.	< L.D.	20	16	95
pixe	0.08	2.94	0.34	49.68	0.14	0.01	1.51	0.01	0.03	45.12	512	60	-	< L.D.	< L.D.	-	7	7	10	< L.D.	16	1	< L.D.	4	6	< L.D.	< L.D.	4	-	< L.D.	-	< L.D.	< L.D.	-	< L.D.	< L.D.
Bordezac						***Bordezac***																		***Bordezac***												
icp	< L.D.	0.34	6.73	13.56	0.14	1.96	0.07	0.18	0.08	74.79	-	-	11.86	192	31.6	8.72	21.0	< L.D.	27.7	9.91	5.87	49.4	72.2	74.8	27.3	81.7	4.71	9.23	0.11	377	6.78	524	14.4	1.96	22.9	258
grotte	< L.D.	< L.D.	12.73	8.08	0.17	2.55	0.03	0.21	0.04	46.16	49	894	176	61	184	1694	< L.D.	34	17	6	7	4	57	13	0	13	4	0	< L.D.	< L.D.	< L.D.	< L.D.	< L.D.	21	78	288
labo	< L.D.	< L.D.	6.38	6.78	0.43	2.40	0.04	0.18	0.03	49.80	508	855	151	89	185	505	13	6	4	7	4	121	54	7	13	5	6	41	< L.D.	< L.D.	< L.D.	< L.D.	< L.D.	1	38	387
pixe	0.09	0.50	11.13	16.52	0.08	2.04	0.07	0.17	0.08	68.89	129	259	-	191	36	< L.D.	7	< L.D.	14	7	3	26	66	69	20	58	7	< L.D.	-	339	-	512	< L.D.	-	18	212

< L.D. en dessous des limites de détections
\- pas de données pour cet élément
1117 valeurs douteuses

	Major elements %									
	Na2O	***MgO***	***Al2O3***	***SiO2***	***P2O5***	***K2O***	***CaO***	***TiO2***	***MnO***	***Fe2O3***
DRN						**DRN**				
ref fiche	2.99	4.4	17.52	52.85	0.25	1.70	7.05	1.09	0.22	9.10
grotte	< L.D.	< L.D.	24.44	37.26	0.28	1.78	3.20	0.48	0.09	8.02
labo	< L.D.	< L.D.	14.67	34.93	0.02	1.78	3.39	0.51	0.10	8.50
pixe	2.42	3.83	18.07	53.48	0.25	1.74	7.30	1.18	0.26	11.27
erreur grotte	-	-	***40***	***30***	***12***	***4***	***55***	***56***	***57***	***12***
erreur labo	-	-	***16***	***34***	***91***	***5***	***52***	***54***	***55***	***7***
erreur pixe	-	-	***3***	***1***	***1***	***2***	***3***	***8***	***-17***	***-24***
BXN						***BXN***				
ref fiche	0.04	0.11	54.21	7.4	0.13	0.05	0.17	2.37	0.05	23.14
grotte	< L.D.	< L.D.	38.57	3.87	0.23	0.05	0.09	1.37	0.04	20.80
labo	< L.D.	< L.D.	33.94	3.01	0.29	0.03	0.08	1.42	0.02	22.50
pixe	< L.D.	0.31	60.32	9.65	0.15	0.06	0.12	2.66	0.05	26.08
erreur grotte	-	-	***28.85***	***48***	***78***	***9***	***45***	***42***	***26***	***10***
erreur labo	-	-	***37.39***	***59***	***120***	***45***	***50***	***40***	***59***	***3***
erreur pixe	-	-	***11.28***	***30***	***14***	***17***	***31***	***12***	***0***	***13***
Bordezac						***Bordezac***				
icp	< L.D.	0.34	6.73	13.56	0.14	1.96	0.07	0.18	0.08	74.79
grotte	< L.D.	< L.D.	12.73	8.08	0.17	2.55	0.03	0.21	0.04	46.16
labo	< L.D.	< L.D.	6.38	6.78	0.43	2.40	0.04	0.18	0.03	49.80
pixe	0.09	0.50	11.13	16.52	0.08	2.04	0.07	0.17	0.08	68.89
erreur grotte	-	-	***89***	***40***	***19***	***31***	***51***	***19***	***53***	***38***
erreur labo	-	-	***5***	***50***	***206***	***23***	***40***	***1***	***60***	***33***
erreur pixe	-	-	***65***	***22***	***44***	***5***	***4***	***4***	***7***	***8***

$\Delta D/D$

	Erreur quanti Major elements en %										Erreur quanti Traces elements en %																									
	Na2O	*MgO*	*Al2O3*	*SiO2*	*P2O5*	*K2O*	*CaO*	*TiO2*	*MnO*	*Fe2O3*	*S*	*Cl*	*Sc*	*V*	*Cr*	*Co*	*Ni*	*Cu*	*Zn*	*Ga*	*Ge*	*As*	*Rb*	*Sr*	*Y*	*Zr*	*Nb*	*Mo*	*In*	*Sb*	*Cs*	*Ba*	*La*	*Hf*	*W*	*Pb*
DRN						**DRN**																		**DRN**												
erreur grotte	-	-	*40*	*30*	*12*	*4*	*55*	*56*	*57*	*12*	*64*	*83*	*98*	*40*	*128*	*1047*	*202*	*43*	*38*	*8*	*64*	-	*37*	*46*	*37*	*28*	*37*	*590*	-	-	-	-	-	*486*	*25*	*6*
erreur labo	-	-	*16*	*34*	*91*	*5*	*52*	*54*	*55*	*7*	*19*	*82*	*356*	*38*	*11*	*324*	*57*	*38*	*33*	*32*	*218*	*1*	*28*	*32*	*68*	*44*	*46*	*2492*	-	-	-	-	-	*59*	*42*	*38*
erreur pixe	-	-	*10*	*4*	*7*	*13*	*16*	*21*	*10*	*8*	*11*	*6*	-	*14*	-	-	*13*	*48*	*19*	*36*	*58*	-	*14*	*14*	*4*	*59*	*14*	-	-	-	-	*64*	-	-	*31*	*13*
BXN						***BXN***																		***BXN***												
erreur grotte	-	-	*29*	*48*	*78*	*9*	*45*	*42*	*26*	*10*	-	-	*86*	*34*	*18*	*2225*	*49*	*2*	*63*	*63*	*40*	*74*	*184*	*63*	*65*	*67*	*55*	*91*	-	-	-	-	-	*24*	*90*	*5*
erreur labo	-	-	*37*	*59*	*120*	*45*	*50*	*40*	*59*	*3*	-	-	*2*	*11*	*16*	*1224*	*47*	*49*	*73*	*64*	*97*	*67*	*64*	*56*	*61*	*55*	*64*	*316*	-	-	-	-	-	*95*	*22*	*4*
erreur pixe	-	-	*11*	*30*	*14*	*17*	*31*	*12*	*0*	*13*	-	-	-	*43*	*8*	-	*6*	*39*	*21*	*19*	*173*	*10*	-	*8*	*7*	*13*	*21*	*69*	-	*213*	-	-	-	-	*167*	*12*
IF-G						***IF-G***																		***IF-G***												
erreur grotte	-	-	*3658*	*30*	*139*	*54*	*38*	*438*	*60*	*35*	*72*	*47*	*81*	*99*	*352*	*3091*	*78*	*59*	*92*	*80*	*547*	*16*	*78*	*99*	*91*	*97*	*69*	*574*	-	-	-	-	-	*136*	*64*	*143*
erreur labo	-	-	*1216*	*16*	*404*	-	*34*	*468*	*90*	*28*	*48*	*165*	*43*	*79*	*193*	*1459*	*87*	*66*	*94*	*91*	*16*	-	*75*	*100*	*77*	*97*	*55*	*2612*	-	-	-	-	-	*462*	*88*	*73*
erreur pixe	-	*56*	*130*	*21*	*129*	*56*	*3*	*61*	*19*	*16*	*46*	*85*	-	-	-	-	*53*	*86*	*93*	-	*742*	*67*	-	*99*	*77*	-	-	*344*	-	-	-	-	-	-	-	-
Bordezac						***Bordezac***																		***Bordezac***												
erreur grotte	-	-	*89*	*40*	*19*	*31*	*51*	*19*	*53*	*38*	-	-	*1380*	*68*	*484*	*19316*	-	-	*37*	*42*	*13*	*92*	*21*	*83*	*99*	*84*	*10*	*96*	-	-	-	-	-	*974*	*238*	*12*
erreur labo	-	-	*5*	*50*	*206*	*23*	*40*	*1*	*60*	*33*	-	-	*1175*	*54*	*485*	*5690*	*40*	-	*85*	*24*	*29*	*146*	*26*	*90*	*51*	*94*	*36*	*342*	-	-	-	-	-	*73*	*65*	*50*
erreur pixe	-	48	65	22	44	5	4	4	7	8	-	-	-	0	14	-	67	-	51	26	49	47	9	8	26	29	42	-	-	10	-	2	-	-	23	18

On the walls

Raw archaeological colouring matter

International standard and geological references

Macroscopic observation

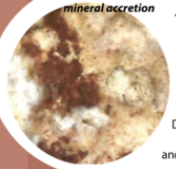

Pictorial matter and mineral accretion

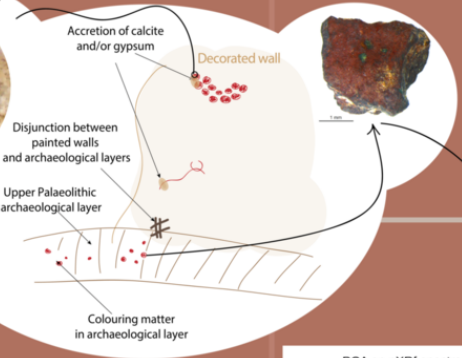

Chemical comparison pXRF, PIXE, ICP

Laboratory

In situ

Comparison of pXRF spectra of colouring matter and bare walls

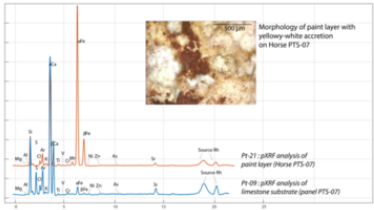

PCA on pXRf spectra of blocks of cohesive colouring matter

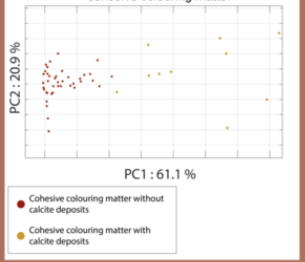

Diagram comparing pXRF – ICP via log ratios of trace elements